

Team Members: Lansong Li, Junning Zhao

School: High School Affiliated to China
Renmin University

Province: Beijing

Country/Region: China Mainland

Supervisor: Yongping Zhang

Title: Rotation Study of Soft Magnetic
Alloy Ring Under Thermo-
Magnetic Interaction

Abstract

This study discovers the phenomenon of bi-directional rotation of soft magnetic alloy ring (SMAR) and conducts a detailed, thorough theoretical analysis on the distribution of forces on SMAR and the pattern of SMAR's rotation. Results show that by utilizing thermo-magnetic effect, a new, efficient way of exploiting solar energy could be achieved.

The magnetization of ferromagnetic material decreases with increasing temperature (below Curie temperature). This phenomenon is called Thermo-Magnetic Effect. Many have utilized this effect to design interesting physics experiments that make SMAR rotate, but none have studied factors that affects the rotation systematically and investigated them theoretically.

An experimental apparatus is constructed during this study which includes SMAR, permanent magnet that generates magnetic field on SMAR and heat source that applied heat at some point of SMAR.

In this study, for the first time, systematic investigations upon physical factors that affect the rotation of SMAR were made by means of both experiment and theoretical analysis. Starting from the magnetic charge model, the circular distribution equation of the magnetic field intensity along the SMAR is established. On this basis, the circular distribution equations of magnetic field intensity gradient and magnetic force density without heat source are derived. From experimental data the curves of circular temperature distribution of SMAR and the relation between relative susceptibility and temperature are fitted out. Finally, the motion model for SMAR under thermo-magnetic effect is established.

Theoretical and experimental studies both demonstrate that without heat source, magnetic forces applied on SMAR are balanced and hence, SMAR does not rotate; When heat source is introduced at one side of the magnet, balance of forces is broken, which in turn, results in the rotation of SMAR.

It is found through theoretical analysis that on each side of the symmetric line, two forces with opposite directions (both clockwise and counter clockwise) exist. This overturns our intuitive understanding.

It is discovered by accident during the experiment that SMAR may rotate either

clockwise or counter clockwise with altering relative position of the magnet to SMAR. Once again it overturns our intuitive understanding. After searching through a large amount of reference materials, we have not found any relevant reports about this phenomenon.

By using our theoretical model, the experimental results of SMAR's bi-directional rotation can be explained perfectly.

Based on our model, if we change the heat source to solar heat, solar energy could be directly converted into controlled, usable mechanical energy and could potentially improve the efficiency of solar energy conversion significantly.

Keywords: Bi-Directional Rotation, Magnet Charge Model, Soft Magnetic Alloy, Magnetic Field

Table of Content

ABSTRACT	I
CHAPTER I INTRODUCTION	1
CHAPTER II EXPERIMENTAL APPARATUS, MEASUREMENT EQUIPMENT AND METHODOLOGY	4
2.1 EXPERIMENTAL APPARATUS CONSTRUCTION	4
2.2 EXPERIMENTAL MEASUREMENT METHODOLOGY AND EQUIPMENT.....	5
2.2.1 Magnetic Field Measurement Method and Equipment	5
2.2.2 Temperature Distribution Measurement Method and Equipment.....	6
2.2.3 SMAR Magnetism and Temperature Distribution Measurement Method and Equipment.....	7
2.2.4 SMAR Rotation Observation and Analysis Method	8
CHAPTER III CONSTRUCTION OF SMAR'S MOTION MODEL UNDER THERMAL AND MAGNETIC INTERACTION	10
3.1 EQUATION OF MAGNETIC FIELD ON SMAR GENERATED BY MAGNET.....	10
3.1.1 Magnetic Charge Model	10
3.1.2 Circular Magnetic Field Generated by Magnetic Charge.....	11
3.1.3 Circular Magnetic Field intensity	11
3.1.4 Circular Magnetic Field Gradient by Magnet	15
3.2 CIRCULAR MAGNETIC FORCE DENSITY DISTRIBUTION OF SMAR.....	16
3.3 TEMPERATURE DISTRIBUTION FITTING FUNCTION OF SMAR.....	18
3.3.1 Susceptibility χ and Temperature T Relation of SMAR	18
3.3.2 Temperature Distribution Function on SMAR	18
3.3.3 Circular Distribution of Relative Magnetic Susceptibility on SMAR.....	18
3.4 MOTION MODEL OF SMAR UNDER THERMO-MAGNETIC INTERACTION.....	19
3.4.1 Magnetic Force Density Distribution of SMAR	19
3.4.2 Total Magnetic Force on SMAR with different Y.....	20
CHAPTER IV SMAR KINETIC EXPERIMENT AND DATA FITTING.....	24
4.1 MEASUREMENT AND ANALYSIS OF MAGNETIC FIELD ON SMAR GENERATED BY MAGNET	24
4.2 MEASUREMENT AND ANALYSIS OF MAGNETIZATION AND TEMPERATURE RELATION ON SMAR.....	27
4.3 MEASUREMENT AND ANALYSIS OF SMAR TEMPERATURE DISTRIBUTION	28
4.4 MOTION OBSERVATION AND ANALYSIS FOR SMAR WITH THERMO-MAGNETIC	

INTERACTION	30
4.4.1 SMAR's Motion Observation and Analysis with Magnet at Y=0.175m.....	30
4.4.2 SMAR's Motion Observation and Analysis with Magnet at Y=0.165m.....	31
4.4.3 SMAR's Motion Observation and Analysis with Magnet at Y=0.155m.....	32
CHAPTER V CONCLUSION AND FUTURE STUDY.....	34
APPENDIX. TABLE OF PHYSICS UNITS AND SIGNS	37
BIBLIOGRAPHY	38
ACKNOWLEDGEMENT.....	39

Chapter I Introduction

Ferromagnetic material is material that contain magnetic domain structure and that only one direction of spontaneous magnetization can occur within one magnetic domain. Soft magnetic alloy is a typical ferro-magnetic material. When external magnetic field exists, soft magnetic alloy shows magnetic properties as a whole. When temperature rises, molecular thermal motion intensifies that results in the reduction of magnetization of soft magnetic alloy. This phenomenon is called thermo-magnetic effect.

Utilizing this effect, people have designed many interesting physical experiments that makes soft magnetic alloy ring (SMAR) rotates. See Fig 1.1. Although these experimental devices differ in structures, they are same in principle. As part of the SMAR is heated, the temperature of this part rises and meanwhile, the magnetic property drops. As a result, the balance of forces applied on the SMAR is broken and the SMAS rotates. Thus, thermo-magnetic effect has a distinctive way (differs from steam engine and thermal power generator) to convert heat energy into mechanical and electrical energy. From there, people has thought of thermo-magnetic engine and thermo-magnetic generator, and did some investigative experiments [3-5].



Fig. 1.1 Demonstrative Apparatus of Thermo-Magnetic Effect

However, from literature, we can only find experiments that are either simply demos of the effect or qualitative descriptions. We have not found any report relating to systematic study or theoretical analysis of various factors that impacts rotation.

This article conducted systematic in-depth analysis and investigation on this interesting physics effects. It is also attempted to establish a motion model for SMAR under Thermo-Magnetic interaction. Fig. 1.2 showed schematic of experimental apparatus used in this work.

However, as we started on our work, we realized that this work is full of challenges.

Firstly, the difference of permeabilities between magnetic materials and the air is far lower than the conductivities between conductor and the air. This cause the calculation accuracy in magnetic circuits is much lower than that in electrical circuits. Secondly, since there are three processes for heat transfer: radiation, convection and conduction, which are existing simultaneously but with different ratio, the quantitative descriptions of the heat transfer are generally very difficult.

According to the above analysis, this work was carried out through the following two paths.

Firstly, starting from the classic electromagnetic theory, the circular distribution equations of the magnetic field intensity and its gradient along the SMAR are established. Furthermore, the circular distribution equation of magnetic force density without heat source is derived; Secondly, in order to simplify the theoretical calculation, the experimental data are fully used to fit two curves of both the circular distribution of temperature and the relation between magnetization and temperature. According to the above two fitted curves, the circular distribution of relative susceptibility is further derived. Based on the results of these two paths, motion model for SMAR under thermo-magnetic effect was finally worked out.

The approach of our work can be shown with flow chart on Fig.1.3.

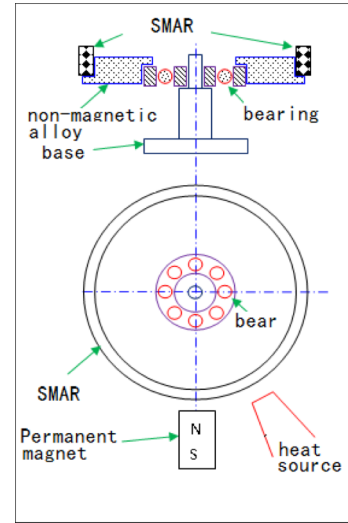
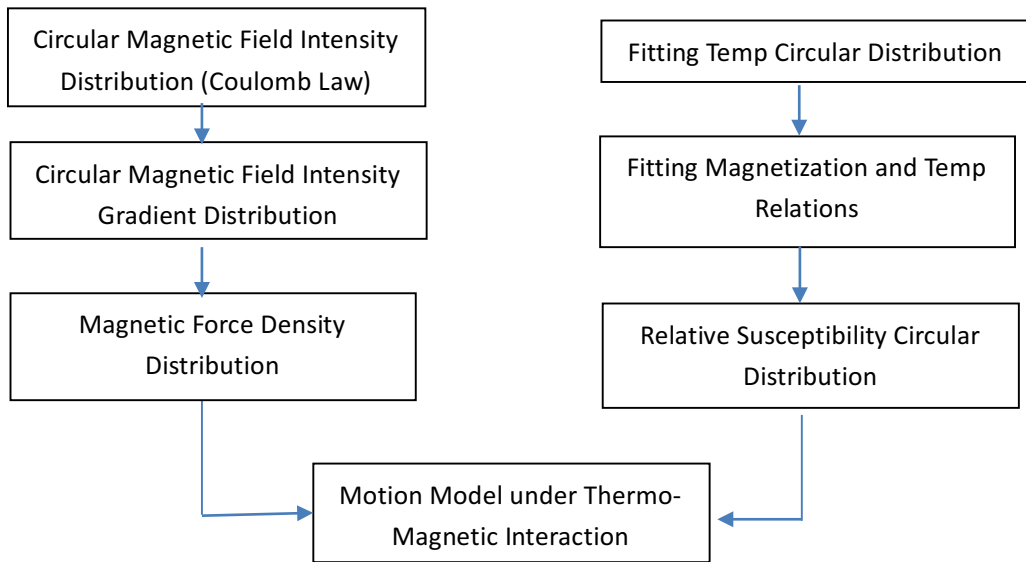


Fig.1.2 Experimental Apparatus

It was discovered accidentally during the study that when distance between magnet and SMAR changes, SMAR's rotation may change directions. In addition, the distance has a balance point, at which point, SMAR does not rotate. Detailed theoretical analysis based on our motion model showed that this new experimental observation can be explained satisfactorily.

Chapter II Experimental Apparatus, Measurement Equipment and Methodology

2.1 Experimental Apparatus Construction

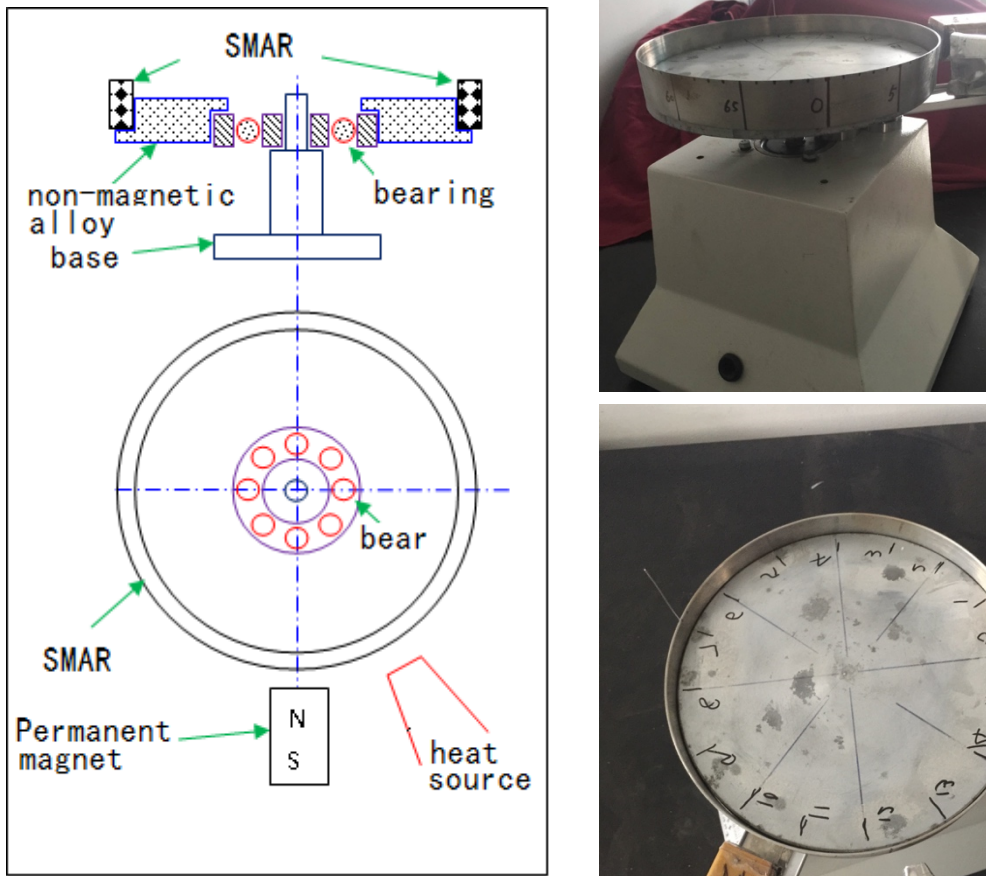


Fig.2.1 Experimental Apparatus schematics and photos

This thermal magnetic rotation experimental platform is constructed entirely with spare parts in the lab, Fig.2.1. Ball bearing was placed on top of a base, ball bearing and non-magnetic alloy base are tightly coupled, Thin soft magnetic alloy (1J36) is attached to the edge of the base. The base is balanced and rotates freely when small force is applied. A permanent magnet is placed outside of the SMAR, Magnet generates a symmetrical magnetic field on the surface of SMAR. On one side of magnet, a fixed heat source is placed to apply heat on SMAR locally.

Magnetic field always attracts soft magnetic material. When heat is not applied, magnetic field on SMAR are symmetrical, thus the force it generated are canceled out. Similarly, total torque is also zero. Therefore, SMAR does not rotate.

When heat source is applied, SMAR's temperature rises in a local area, Heat

transfers from the local area outwards and generated temperature gradient. Due to sensitive nature of magnetization to temperature, this temperature gradient can result in significant magnetization differential of SMAR. This change disturbed balance of magnetic force on SMAR, total magnetic force is no longer symmetrically distributed, a rotary torque is generated. Thus, SMAR started rotating under this torque.

To quantify SMAR's motion, we set certain experimental parameters, listed below, for the platform.

- (1) Rotation platform (non-magnetic alloy, base plate and ball bearing): Rotation platform is a recycled polishing machine. Friction in ball bearing are ignored for this calculation.
- (2) Magnet: Block Nd-Fe-B Rare Earth Magnet is used. (60mm x 30mm x 30mm). Magnet and SMAR are on the same height. N pole is placed closed to SMAR surface and placed along the radius. The distance between N and center of the platform varies during the experiments.
- (3) Soft Magnetic Alloy Ring (SMAR): SMAR made of 1J36 metallic soft magnetic alloy. The magnetization of 1J36 alloy varies linearly with the experimental temperature (room-temperature \sim 200 degree in Celsius). Its Curie temperature is about 230°C. SMAR has radius R of 114mm, thickness of 1mm and height of 30mm.
- (4) Fixed heat source: Electro-Resistance heat source, and a blower as a heat transfer device. Heat source is place on the right side and 12 degree off of magnet with 5 mm away from SMAR surface.

2.2 Experimental Measurement Methodology and Equipment

2.2.1 Magnetic Field Measurement Method and Equipment

LZ-610H portable Tesla Meter is used to measure magnetic circular distribution on SMAR. Measurement equipment is pictured in Fig.2.3.

Measurement Method: Divide the round base to equal part through center. Place the magnet (10 and 20mm) away from the surface. See Fig.2.2. Tesla Meter is used to probe and measure the magnetic field. The probe is placed tangent direction along a ring of same size with SMAR and perpendicular to the radius. The range of measurement is from 0 degree to 57 degree on each direction. Once one set of

measurement is completed, the platform is turned 180 degrees, Magnet is also turned independently for comparison measurement. The measured data set are analyzed, and compared with computational model.

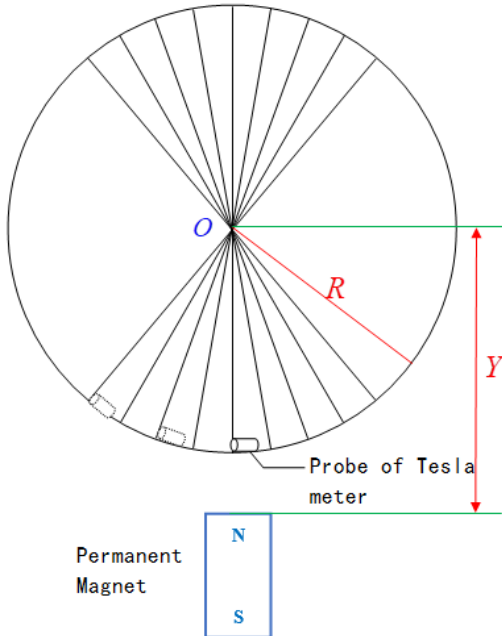


Fig.2.2 Schematic of Magnetic Field Measurement



Fig.2.3 LZ-610H Portable Tesla Meter

2.2.2 Temperature Distribution Measurement Method and Equipment

AS872 portable infra-red thermometer is utilized to measure SMAR surface temperature. Fig.2.4 is schematic for temperature distribution measurement. Fig.2.5 shows AS872 Portable Infra-Red Thermometer.

Measurement method: The heat source with fixed position is turned on continuously. Infra-Red thermometer is placed 90 degrees to the right of magnet. SMAR attached to the non-magnetic base is divided to 60 equal parts. Data is collected via rotating the ring quickly to move a particular point to effective measurement region of thermometer. Once a data point is collected, SMAR is rotated back to original location, and heat up for 30 seconds before next point is measured. ± 90 degree is measured around the heat source. Before starting the measurement, move the magnet far away. During the measurement, position of heat source and thermometer are fixed.

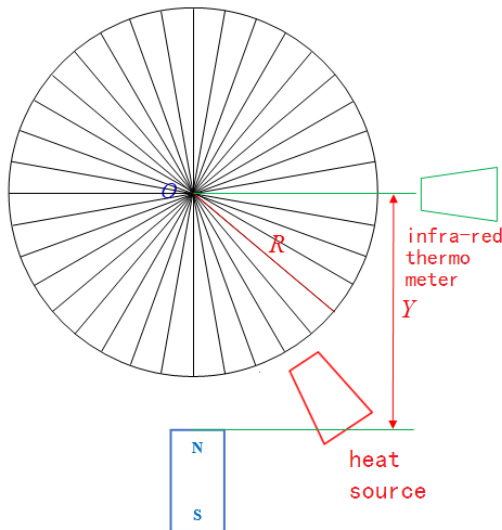


Fig.2.4 Schematic of SMAR Temp Distribution Measurement



Fig.2.5 Portable Infra-Red Thermometer

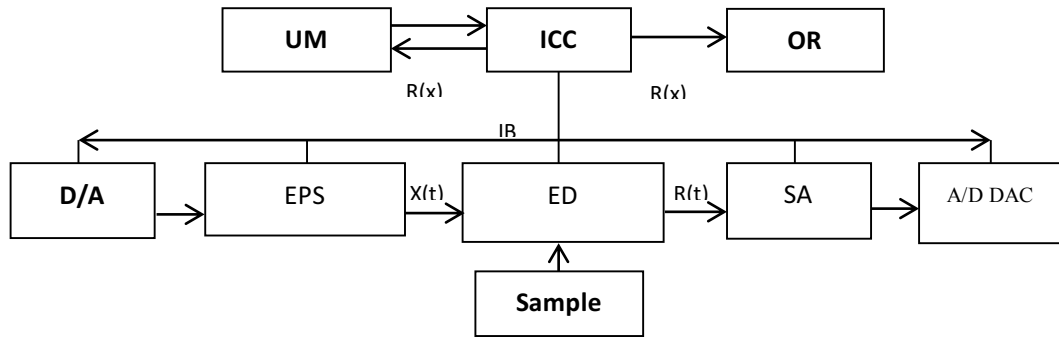
2.2.3 SMAR Magnetism and Temperature Distribution Measurement Method and Equipment

The sample of SMAR used in this experiment is 1J36 alloy with size of $\Phi 32/40 \times 5\text{mm}$. The relationship between magnetization and temperature is determined experimentally.

Measurement is made on NIM-2000S soft magnetic material DC measurement system (Fig.2.6). This system consists of industrial control computer, digital-to-analog convertor, analog-to-digital data collector, current distributor integrator and excitation magnetic field power supply.



Fig. 2.6 NIM-2000S Soft Magnetic Material DC Magnetic Measurement System



UM==Upper Microcomputer; ICC== Industrial Control Computer; OR==Output Result; IB==Interface Bus;
 D/A== D/A Converter; EPS==Excitation Power Supply; ED==Excitation Device; SA== Sensor Amplifier;
 A/D DAC==Data Acquisition Card

Fig.2.7 Theoretic Diagram of Magnetic Materials Measurement System

Fig.2.7 is diagram of magnetic materials measurement system. This experiment utilized impact measurement of 1J36 alloy's B_{3200} , which is magnetization when $H=3200\text{A/m}$. Sample was placed in box furnace with testing temperature between room temperature to 200C. At each test temperature, sample was kept for 30 mins before test was conducted to ensure that test temperature is stable. Three test samples are used to test, the average of the three sample results are used in analysis.

The relation of Magnetic flux density B , Magnetic Field Strength H and Magnetization M are:

$$B = \mu_0 H + \mu_0 M$$

In which, $\mu_0 = 4\pi \times 10^{-7} \text{ SI}$ is permeability in vacuum, and $\mu_0 M$ is magnetic polarization strength.

2.2.4 SMAR Rotation Observation and Analysis Method

With fixed heat source, varying distance between magnet and center of platform, experimental data and computational model are used to verify against each other.

Observation of SMAR rotation is through photo and video recording. Each controlling parameter is recorded in detail. To limit other factors' effect, only magnetic distances are changed. Other parameters are not changed. Detailed measurement methods are:

- (1) Firstly, SMAR is attached to the test platform. SMAR can rotate with tiny disturbance.

- (2) Magnet is placed at one side of SMAR, and on the same height as SMAR with pole N close and parallel to the SMAR surface. Measurement and recording of pole N and center of platform Y is shown in Fig.2.8(A).
- (3) Fixed heat source is 12 degree to the right of magnet, and is 5mm away from SMAR. Blower is used to accelerate heat transfer to SMAR.
- (4) Adjusting Y to $Y \geq 0.175\text{m}$, applying heat for 5min, observe and record SMAR's rotation, Fig.2.8(B). Stop heat source and cool test platform to room temperature, and prepare for follow-on tests.
- (5) Adjusting Y to $Y = 0.165\text{m}$, applying heat for 5min, observe and record SMAR's rotation, Fig. 2.8(C). Stop heat source and cool test platform to room temperature, and prepare for follow-on tests.
- (6) Adjusting Y to $Y \leq 0.155\text{m}$, applying heat for 5min, observe and record SMAR's rotation, Fig. 2.8(D). Stop heat source and cool test platform to room temperature, and complete the tests.

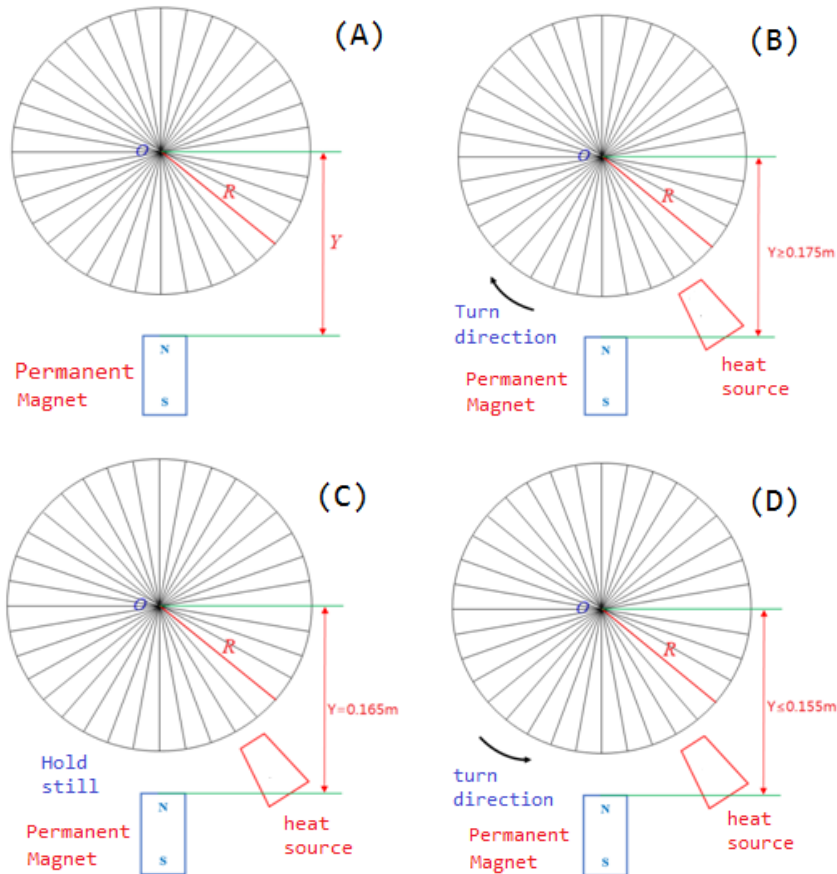


Fig 2.8 Schematics for SMAR motion state

Chapter III Construction of SMAR's Motion Model

Under Thermal and Magnetic Interaction

3.1 Equation of Magnetic Field on SMAR Generated by Magnet

3.1.1 Magnetic Charge Model

Assuming inside of magnet is homogenously magnetized, its magnetization is M . Because of uniformly magnetized, $\nabla \cdot M = 0$. Based on magnetic charge definition $\rho_m = -\mu_0 \nabla \cdot M$, magnetic charge within magnet is zero, magnetic charge only exists at magnet's surface.

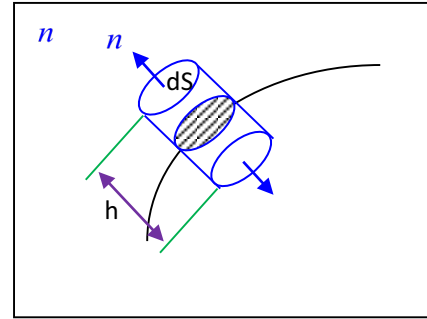


Fig.3.1 Magnetic Surface

As shown in the Fig.3.1, pick a small volume V from magnet's surface, area as dS , thickness as h . When $h \rightarrow 0$, the magnet charge density can be derived from

divergence $\nabla \cdot M = \lim_{V \rightarrow 0} \frac{1}{V} \iint_S M \cdot dS$:

$$\begin{aligned}\rho_m &= -\mu_0 \lim_{V \rightarrow 0} \frac{1}{V} \iint_S M \cdot dS \\ &= -\mu_0 \lim_{V \rightarrow 0} \frac{1}{V} (M_{\text{outside}} \cdot dS_{\text{outside}} + M_{\text{inside}} \cdot dS_{\text{inside}} + M_{\text{side}} \cdot dS_{\text{side}})\end{aligned}$$

since $M_{\text{outside}} = 0$, $M_{\text{inside}} = M$, $dS_{\text{side}} \rightarrow 0$, so

$$\rho_m = -\mu_0 \lim_{V \rightarrow 0} \frac{1}{V} M \cdot dS = -\mu_0 \lim_{h \rightarrow 0} \frac{dS \cdot M \cdot n}{h \cdot dS} = -\mu_0 \lim_{h \rightarrow 0} \frac{M \cdot n}{h}$$

And $\rho_m = \frac{q_m}{V} = \frac{\sigma_m \cdot dS}{h \cdot dS} = \frac{\sigma_m}{h}$, that is, $\sigma_m = \rho_m h$, σ_m is surface density of magnetic charge. Note n is set as volume V 's outward direction, volume $V \rightarrow 0$. If set n as magnet surface outward direction, combined with above equation:

$$\sigma_m = \mu_0 M \cdot n \quad (3-1)$$

Thus, magnetic charge on magnet's end surface is:

$$q_m = \sigma_m S = \mu_0 M_p S \quad (3-2)$$

In the equation, M_p is magnet's magnetization, S as surface area of end surface.

3.1.2 Circular Magnetic Field Generated by Magnetic Charge

Based on magnetic charge's Coulomb Law, static magnetic field generated by magnetic charge q_m is:

$$H = \frac{1}{4\pi\mu_0} \cdot \frac{q_m}{r^2} \hat{r} \quad (3-3)$$

put (3-2) into (3-3), magnetic field intensity generated by magnetic charge is:

$$H = \frac{M_p S}{4\pi r^2} \hat{r} \quad (3-4)$$

3.1.3 Circular Magnetic Field intensity

For magnetic ring shaped like a cylinder, when ring is magnetized, due to demagnetization field, demagnetization factor along radial direction $N \approx 1$, Only circular and axial directions are magnetized. In addition, see Fig.3.2, point P located at the vertical center of the ring. Circular magnetic field at P is used to represent that of small area along axial direction with P at the center. Since magnetic field direction for this area is the same as P, a two-dimentional approximation is chosen for this study.

Fig.3.3, polar coordinate is used where C is center of magnetic ring, is also origin for polar coordinates; R is radius of magnetic ring, Y is distance of C and end surface of magnet end surface. S is magnet source on end surface of magnet. Coordinate's setting showed in figure 3.3.

On magnetic ring, point P's coordinates are $P(R, \theta)$, magnet charge point S has coordinate of $S(Y, 0)$, from cosine theorem:

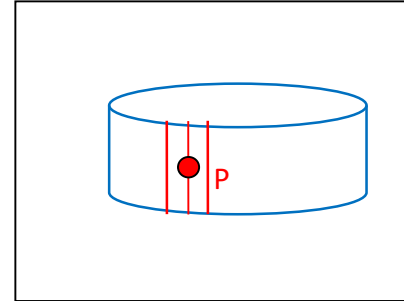


Fig.3.2 Schematic of SMAR

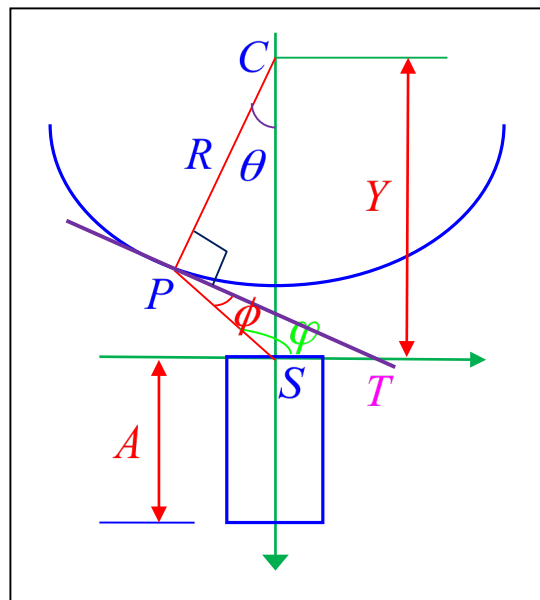


Fig. 3.3 Magnet and SMAR

$$PS^2 = CP^2 + CS^2 - 2 \cdot CP \cdot CS \cos \angle PCS$$

Set $PS = r$, $CP = R$, $CS = Y$, $\angle PCS = \theta$, then:

$$r^2 = R^2 + Y^2 - 2RY \cos \theta \quad (3-5)$$

Tangent of Circle C through point P crosses horizontal line where S is on at T, set the cross angle between PS and PT be ϕ , that is $\angle SPT = \phi$, $\angle PST = \varphi$. Since $\angle STP = \theta$, $\phi = 180^\circ - \varphi - \theta$, then:

$$\cos \phi = \cos(180^\circ - \varphi - \theta) = -\cos(\varphi + \theta) = -\cos \varphi \cos \theta + \sin \varphi \sin \theta \quad (3-6)$$

From this geometric figure, we get

$$\sin \varphi = \frac{Y - R \cos \theta}{\sqrt{R^2 + Y^2 - 2RY \cos \theta}}, \quad \cos \varphi = \frac{R \sin \theta}{\sqrt{R^2 + Y^2 - 2RY \cos \theta}} \quad (3-7)$$

Bring (3-7) into (3-6):

$$\cos \phi = \frac{-R \sin \theta \cos \theta + (Y - R \cos \theta) \sin \theta}{\sqrt{R^2 + Y^2 - 2RY \cos \theta}} = \frac{Y \sin \theta - R \sin 2\theta}{\sqrt{R^2 + Y^2 - 2RY \cos \theta}} \quad (3-8)$$

Magnetic Field's tangent component $H_\theta(\theta)$ generated by magnetic charge S at point P can be derived from (3-4) :

$$H_\theta(\theta) = \frac{M_p S}{4\pi} \cdot \frac{\cos \phi}{r^2}$$

Bring (3-5) and (3-8) into above equation:

$$H_\theta(\theta) = \frac{M_p S}{4\pi} \cdot \frac{Y \sin \theta - R \sin 2\theta}{(R^2 + Y^2 - 2RY \cos \theta)^{3/2}}$$

Set proportional factor $\frac{Y}{R} = \lambda$, above equation becomes:

$$H_\theta(\theta, \lambda) = \frac{M_p S}{4\pi R^2} \cdot \frac{\lambda \sin \theta - \sin 2\theta}{(1 + \lambda^2 - 2\lambda \cos \theta)^{3/2}} \quad (3-9)$$

Set magnetic field source as area dS and located at θ' , circular magnetic field is derived from (3-9):

$$dH_\theta(\theta') = \frac{M_p dS}{4\pi R^2} \cdot \frac{\lambda \sin(\theta - \theta') - \sin 2(\theta - \theta')}{[1 + \lambda^2 - 2\lambda \cos(\theta - \theta')]^{3/2}} \quad (3-10)$$

Convert from area unit dS to angle unit:

$$dS = \frac{S_p}{2\beta} d\theta'$$

In which, S_p is area for magnetic end source, angle θ' has range of $[-\beta, \beta]$, $\beta \approx \frac{D}{Y}$,

thus (3-10) becomes:

$$dH_\theta(\theta') = \frac{M_p S_p}{4\pi R^2} \cdot \frac{1}{2\beta} \frac{\lambda \sin(\theta - \theta') - \sin 2(\theta - \theta')}{[1 + \lambda^2 - 2\lambda \cos(\theta - \theta')]^{3/2}} d\theta' \quad (3-11)$$

Integral of function of $f(\theta') = \frac{\lambda \sin(\theta - \theta') - \sin 2(\theta - \theta')}{[1 + \lambda^2 - 2\lambda \cos(\theta - \theta')]^{3/2}}$ is:

$$\int_{-\beta}^{\beta} f(\theta') d\theta' = \int_{-\beta}^{\beta} \frac{\lambda \sin(\theta - \theta') - \sin 2(\theta - \theta')}{[1 + \lambda^2 - 2\lambda \cos(\theta - \theta')]^{3/2}} d\theta' \quad (3-12)$$

With replacement, set $\theta - \theta' = \alpha$, α has a range of $\alpha \in [\theta - \beta, \theta + \beta]$:

$$f(\alpha) d\alpha = \frac{\lambda \sin \alpha - \sin 2\alpha}{[1 + \lambda^2 - 2\lambda \cos \alpha]^{3/2}} d\alpha = \frac{1}{2} \cdot \frac{\lambda - 2 \cos \alpha}{[1 + \lambda(\lambda - 2 \cos \alpha)]^{3/2}} \cdot d(\lambda - 2 \cos \alpha)$$

Set $z = \lambda - 2 \cos \alpha$, above integral becomes:

$$\begin{aligned} \frac{1}{2} \int \frac{z}{(1 + \lambda z)^{3/2}} dz &= \frac{1}{2} \frac{1}{\lambda^2} \int \left[\frac{1}{(1 + \lambda z)^{1/2}} - \frac{1}{(1 + \lambda z)^{3/2}} \right] d(1 + \lambda z) \\ &= \frac{1}{2} \frac{1}{\lambda^2} \left[2\sqrt{1 + \lambda z} + \frac{2}{\sqrt{1 + \lambda z}} \right] = \frac{1}{\lambda^2} \cdot \frac{2 + \lambda z}{\sqrt{1 + \lambda z}} \end{aligned}$$

So

$$\frac{1}{\lambda^2} \cdot \left[\frac{2 + \lambda(\lambda - 2 \cos \alpha)}{\sqrt{1 + \lambda(\lambda - 2 \cos \alpha)}} \right]_{\theta-\beta}^{\theta+\beta} = \frac{1}{\lambda^2} \left[\frac{2 + \lambda^2 - 2\lambda \cos(\theta + \beta)}{\sqrt{1 + \lambda^2 - 2\lambda \cos(\theta + \beta)}} - \frac{2 + \lambda^2 - 2\lambda \cos(\theta - \beta)}{\sqrt{1 + \lambda^2 - 2\lambda \cos(\theta - \beta)}} \right]$$

Set

$$\Phi(\lambda, \theta) = \frac{1}{2\beta\lambda^2} \left[\frac{2 + \lambda^2 - 2\lambda \cos(\theta + \beta)}{\sqrt{1 + \lambda^2 - 2\lambda \cos(\theta + \beta)}} - \frac{2 + \lambda^2 - 2\lambda \cos(\theta - \beta)}{\sqrt{1 + \lambda^2 - 2\lambda \cos(\theta - \beta)}} \right] \quad (3-13)$$

Integral of magnetic field on magnet's end surface (3-11) can be described:

$$H_\theta(\theta, \lambda) = \frac{M_p S_p}{4\pi R^2} \cdot \Phi(\lambda, \theta) \quad (3-14)$$

Similarly, set $Y' = (Y + A)$, $\frac{Y'}{R} = \lambda'$, contribution from the other end surface is:

$$H_\theta(\theta, \lambda') = -\frac{M_p S_p}{4\pi R^2} \cdot \Phi(\lambda', \theta) \quad (3-15)$$

In which:

$$\Phi(\lambda', \theta) = \frac{1}{2\beta' \lambda'^2} \left[\frac{2 + \lambda'^2 - 2\lambda' \cos(\theta + \beta')}{\sqrt{1 + \lambda'^2 - 2\lambda' \cos(\theta + \beta')}} - \frac{2 + \lambda'^2 - 2\lambda' \cos(\theta - \beta')}{\sqrt{1 + \lambda'^2 - 2\lambda' \cos(\theta - \beta')}} \right] \quad (3-16)$$

where

$$\beta' = \frac{D}{Y'} = \frac{D}{Y + A}$$

Combined contribution from both end surfaces:

$$H_\theta(\theta) = \frac{M_p S_p}{4\pi R^2} [\Phi(\lambda, \theta) - \Phi(\lambda', \theta)] \quad (3-17)$$

This is total circular magnetic field intensity from both end surfaces.

Set $R = 0.114m$, $Y = 0.150m$, $A = 0.060m$, $D = 0.015m$, then $\lambda = 1.3158$, $\lambda' = 1.8421$, $\beta = \frac{0.015}{0.150} = 0.1$, $\beta' = \frac{0.015}{0.150 + 0.060} = 0.0714$. Circular magnetic field intensity distribution with $\frac{M_p S}{4\pi R^2}$ as unit is shown in Fig.3.4.

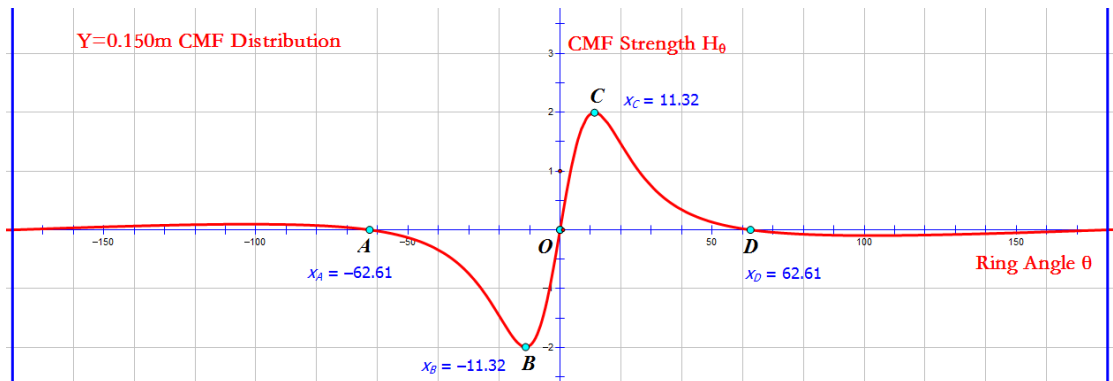


Fig. 3.4 SMAR's Circular Magnetic Field (CMF) intensity Distribution at $Y = 0.150m$

Horizontal axis is the angle along SMAR, and vertical axis is circular magnetic field intensity. When curve is above the horizontal axis, magnetic field intensity is positive, indicating counter clockwise magnetic field; When curve is below the axis, field intensity is negative, indicating clockwise magnetic field. There are two peak value at $\theta = \pm 11.32^\circ$; two zero crossing point at $\theta = \pm 62.61^\circ$.

3.1.4 Circular Magnetic Field Gradient by Magnet

Get derivative of (3-17):

$$\frac{1}{R} \frac{\partial H_\theta(\theta)}{\partial \theta} = \frac{M_p S_p}{4\pi R^3} \left[\frac{\partial \Phi(\lambda, \theta)}{\partial \theta} - \frac{\partial \Phi(\lambda', \theta)}{\partial \theta} \right]$$

In which from (3-13):

$$\begin{aligned} \frac{\partial \Phi(\lambda, \theta)}{\partial \theta} &= \frac{1}{2\beta\lambda^2} \frac{\partial}{\partial \theta} \left[\frac{2 + \lambda^2 - 2\lambda \cos(\theta + \beta)}{\sqrt{1 + \lambda^2 - 2\lambda \cos(\theta + \beta)}} - \frac{2 + \lambda^2 - 2\lambda \cos(\theta - \beta)}{\sqrt{1 + \lambda^2 - 2\lambda \cos(\theta - \beta)}} \right] \\ &= \frac{1}{2\beta\lambda^2} \frac{\partial}{\partial \theta} \left[\sqrt{1 + \lambda^2 - 2\lambda \cos(\theta + \beta)} + \frac{1}{\sqrt{1 + \lambda^2 - 2\lambda \cos(\theta + \beta)}} \right] \\ &\quad - \frac{1}{2\beta\lambda^2} \frac{\partial}{\partial \theta} \left[\sqrt{1 + \lambda^2 - 2\lambda \cos(\theta - \beta)} + \frac{1}{\sqrt{1 + \lambda^2 - 2\lambda \cos(\theta - \beta)}} \right] \\ &= \frac{1}{2\beta} \left[\frac{\lambda \sin(\theta + \beta) - \sin 2(\theta + \beta)}{(1 + \lambda^2 - 2\lambda \cos(\theta + \beta))^{3/2}} - \frac{\lambda \sin(\theta - \beta) - \sin 2(\theta - \beta)}{(1 + \lambda^2 - 2\lambda \cos(\theta - \beta))^{3/2}} \right] \end{aligned}$$

Similarly:

$$\frac{\partial \Phi(\lambda', \theta)}{\partial \theta} = \frac{1}{2\beta'} \left[\frac{\lambda' \sin(\theta + \beta') - \sin 2(\theta + \beta')}{(1 + \lambda'^2 - 2\lambda' \cos(\theta + \beta'))^{3/2}} - \frac{\lambda' \sin(\theta - \beta') - \sin 2(\theta - \beta')}{(1 + \lambda'^2 - 2\lambda' \cos(\theta - \beta'))^{3/2}} \right]$$

set:

$$G(\lambda, \theta) = \frac{1}{2\beta} \left[\frac{\lambda \sin(\theta + \beta) - \sin 2(\theta + \beta)}{(1 + \lambda^2 - 2\lambda \cos(\theta + \beta))^{3/2}} - \frac{\lambda \sin(\theta - \beta) - \sin 2(\theta - \beta)}{(1 + \lambda^2 - 2\lambda \cos(\theta - \beta))^{3/2}} \right] \quad (3-18)$$

$$G(\lambda', \theta) = \frac{1}{2\beta'} \left[\frac{\lambda' \sin(\theta + \beta') - \sin 2(\theta + \beta')}{(1 + \lambda'^2 - 2\lambda' \cos(\theta + \beta'))^{3/2}} - \frac{\lambda' \sin(\theta - \beta') - \sin 2(\theta - \beta')}{(1 + \lambda'^2 - 2\lambda' \cos(\theta - \beta'))^{3/2}} \right] \quad (3-19)$$

Circular magnetic field gradient by magnet is:

$$\frac{1}{R} \frac{\partial H_\theta(\theta)}{\partial \theta} = \frac{M_p S_p}{4\pi R^3} [G(\lambda, \theta) - G(\lambda', \theta)] \quad (3-20)$$

Set $R = 0.114m$, $Y = 0.150m$, $A = 0.060m$, $D = 0.015m$, then $\lambda = 1.3158$,

$$\lambda' = 1.8421, \quad \beta = \frac{0.015}{0.150} = 0.1, \quad \beta' = \frac{0.015}{0.150 + 0.060} = 0.0714. \text{ Circular magnetic field}$$

gradient is shown in Fig 3.5 with $\frac{M_p S_p}{4\pi R^3}$ as unit.

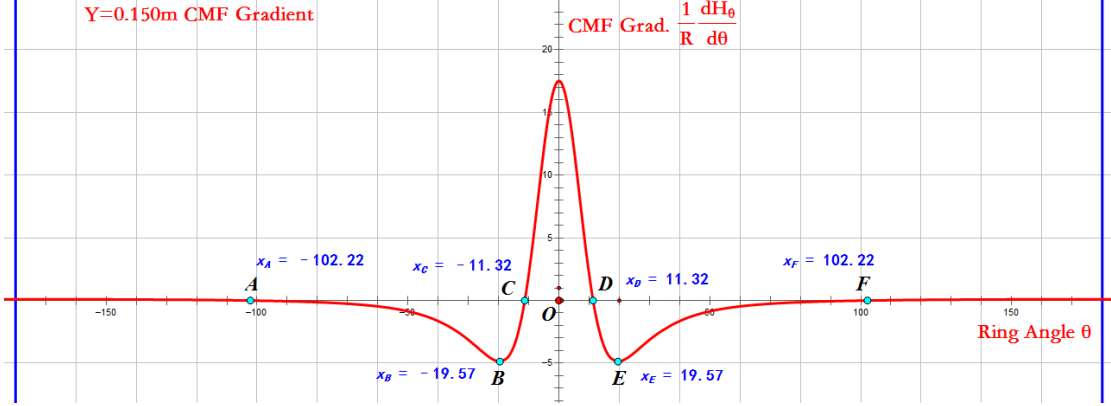


Fig. 3.5 SMAR's Circular Magnetic Gradient (CMF Grad.) at Y=0.150m

Circular magnetic field gradient at magnetic ring has two extreme value and two zero-cross points besides $\theta = 0^\circ$. Two extreme values appear at $\theta = \pm 19.57^\circ$, and a peak at $\theta = 0^\circ$. Two near zero-cross points at $\theta = \pm 11.32^\circ$, and far zero-cross points at $\theta = \pm 102.22^\circ$.

3.2 Circular Magnetic Force Density Distribution of SMAR

At P, magnetic energy density is $E_m = \frac{1}{2} H \cdot B$. For magnetic media

$B = \mu_0 (H + M)$, thus:

$$E_m = \frac{1}{2} H \cdot B = \frac{1}{2} \mu_0 H \cdot (H + M) = \frac{1}{2} \mu_0 H^2 + \frac{1}{2} \mu_0 H M = \frac{1}{2} \mu_0 H^2 + \frac{1}{2} \mu_0 \chi H^2$$

In which $\chi \gg 1$ is susceptibility of magnetic media. First part of the equation is the energy density of magnetic field, and second part is energy density of magnetic media. Main contributor of force on magnetic media is the second part.

Susceptibility of soft magnetic material is a function of magnetic field intensity H and temperature T. Its hysteresis loop is a thin loop. To simplify the model, we approximate the loop as a line curve, and at certain range of magnetic field, it is considered linear. That is, susceptibility χ is a function of temperature T and does not change with magnetic field intensity. With these, circular component of force on magnetic media unit volume is:

$$f_\theta(\theta) = -(\Delta E)_\theta = -\frac{1}{R} \frac{\partial}{\partial \theta} \left(\frac{1}{2} \mu_0 \chi H_\theta^2 \right) = -\frac{\mu_0 \chi}{R} H_\theta \frac{dH_\theta}{d\theta} \quad (3-21)$$

f_θ is circular magnetic force density. The negative sign only indicates attraction force along magnetic pole direction. Since we focus on circular direction force, negative sign is removed from here on.

Bring(3-17) and(3-20) into (3-21), circular magnetic density distribution is:

$$f_\theta(\theta) = \frac{\mu_0}{R} \left(\frac{M_p S_p}{4\pi R^2} \right)^2 \chi [\Phi(\lambda, \theta) - \Phi(\lambda', \theta)] [G(\lambda, \theta) - G(\lambda', \theta)] \quad (3-22)$$

Set $R = 0.114m$, $Y = 0.150m$, $A = 0.060m$, $D = 0.015m$, then $\lambda = 1.3158$,

$$\lambda' = 1.8421, \beta = \frac{0.015}{0.150} = 0.1, \beta' = \frac{0.015}{0.150 + 0.060} = 0.0714. \text{ Circular magnetic}$$

force density is shown in Fig. 3.6 with $\frac{\mu_0 \chi}{R} \left(\frac{M_p S_p}{4\pi R^2} \right)^2$ as unit.

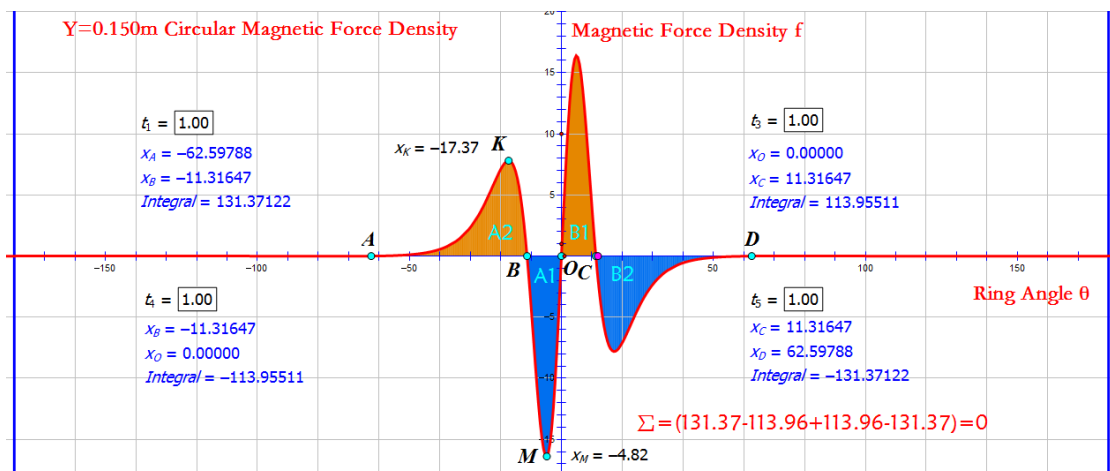


Fig.3.6 SMAR's Circular Magnetic Density Distribution at $Y=0.150m$

Calculation results show there are two zero-cross points at $\theta = \pm 11.32^\circ$ besides $\theta = 0^\circ$. There are four extreme values on the curve. They are at $\theta = \pm 4.82^\circ$ and $\theta = \pm 17.37^\circ$ respectively.

There are four regions on the magnetic force density curve, they are denoted as A1, A2, B1 and B2 (as shown in the fig.3.6). Their area represents magnetic force on the region. Sum of all the areas represents total force applied on the SMAR. Torque on SMAR is total force multiplied by SMAR's radius. Torque and force have same direction. Thus, this force/torque direction determines ring rotation direction.

In the graph, curve below horizontal line is negative, indicates that the area has force of negative θ direction, that is clockwise. Similarly, curve above horizontal line is positive, indicates that the area has force of positive θ direction, which is counter clockwise direction. There are three zero-cross point close to center point where

$\theta = 0^\circ$. They are at $\theta = 0^\circ$ and $\theta = \pm 11.32^\circ$ respectively.

3.3 Temperature Distribution Fitting Function of SMAR

3.3.1 Susceptibility χ and Temperature T Relation of SMAR

Magnetic polarization strength $\mu_0 M_s$ and temperature T are measured experimentally, and derived Magnetization M_s and Temperature T relations. This represents susceptibility of SMAR χ and Temperature T relation:

Measurement results indicate: at the experimental temperature range, the relationship between Magnetization M_s and Temperature T for SMAR used in this study is close to linear. Thus, this study used a linear fitting function:

$$\chi(T) = \gamma(1 - \alpha T) \quad (3-23)$$

Experimental results and data process are shown in Chapter IV section 4.2.

3.3.2 Temperature Distribution Function on SMAR

Temperature distribution on SMAR under single local heat source is measured. The results indicate that temperature distribution is a single peak symmetrical curve. Following is the fitting function for this curve:

$$T(\theta) = T_0 \left[(\theta + b)^{\frac{1}{3}} - (\theta - b)^{\frac{1}{3}} \right] + T_r \quad (3-24)$$

In the function, temperature peak is located at $\theta_0 = 0^\circ$. T_0 is a undetermined factor, b is a width factor, T_r is background temperature.

When temperature peak is at $\theta_0 \neq 0^\circ$, (3-24) becomes:

$$T(\theta) = T_0 \left[(\theta - \theta_0 + b)^{\frac{1}{3}} - (\theta - \theta_0 - b)^{\frac{1}{3}} \right] + T_r \quad (3-25)$$

Experimental results and data processing are shown in Chapter IV section 4.3.

3.3.3 Circular Distribution of Relative Magnetic Susceptibility on SMAR

From (3-23) and (3-25), we can derive $\chi = \chi(\theta)$, circular distribution of relative magnetic susceptibility on SMAR.

Bring (3-25) into (3-23):

$$\begin{aligned}
\chi(\theta) &= \gamma [1 - \alpha T(\theta)] = \gamma - \gamma \alpha T(\theta) \\
&= \gamma - \gamma \alpha \left\{ T_0 \left[(\theta - \theta_0 + b)^{\frac{1}{3}} - (\theta - \theta_0 - b)^{\frac{1}{3}} \right] + T_r \right\} \\
&= \gamma - \gamma \alpha T_0 \left[(\theta - \theta_0 + b)^{\frac{1}{3}} - (\theta - \theta_0 - b)^{\frac{1}{3}} \right] - \gamma \alpha T_r \\
&= \gamma (1 - \alpha T_r) \left\{ 1 - \frac{\alpha T_0}{1 - \alpha T_r} \left[(\theta - \theta_0 + b)^{\frac{1}{3}} - (\theta - \theta_0 - b)^{\frac{1}{3}} \right] \right\} \quad (3-26)
\end{aligned}$$

Pick $T_r = 313K$, $T_0 = 12$, $\alpha = 0.00183$, $\gamma = 777$, $\theta_0 = 12$, $b = 16$, place them into (3-26) to get relative susceptibility χ distribution function with respect to θ .

$$\chi(\theta) = 332 \left\{ 1 - 0.0514 \left[(\theta + 4)^{\frac{1}{3}} - (\theta - 28)^{\frac{1}{3}} \right] \right\} \quad (3-27)$$

Distribution curve from (3-27) is shown in Fig.3.7.

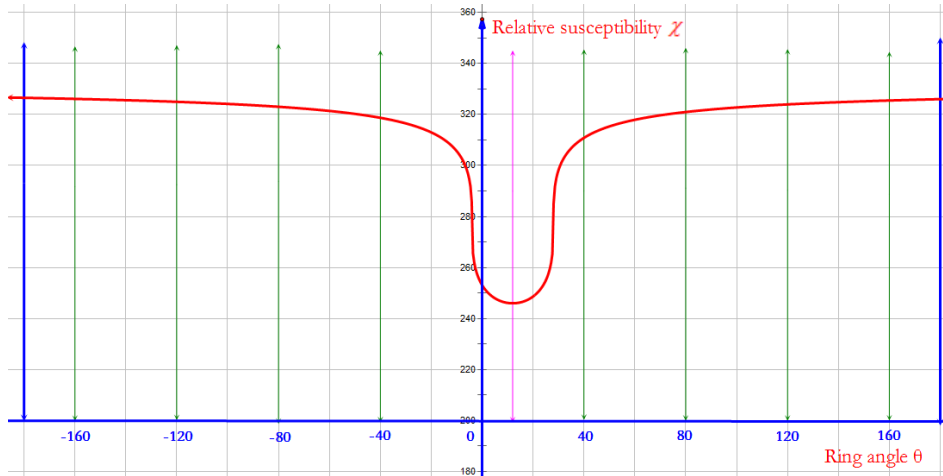


Fig. 3.7 Relative Magnetic Susceptibility Distribution on SMAR

Fig. 3.7 shows that susceptibility on SMAR is lower when temperature is higher, and higher when temperature is lower.

3.4 Motion model of SMAR under Thermo-Magnetic Interaction

3.4.1 Magnetic Force Density Distribution of SMAR

Bring relative susceptibility distribution equation (3-26) into equation (3-22), we get the circular magnetic force density on SMAR:

$$f_\theta(\theta) = k \left\{ 1 - \frac{\alpha T_0}{1 - \alpha T_r} \left[(\theta - \theta_0 + b)^{\frac{1}{3}} - (\theta - \theta_0 - b)^{\frac{1}{3}} \right] \right\} [\Phi(\lambda, \theta) - \Phi(\lambda', \theta)] [G(\lambda, \theta) - G(\lambda', \theta)] \quad (3-28)$$

In which,

$$k = \frac{\mu_0}{R} \left(\frac{M_P S_P}{4\pi R^2} \right)^2 \gamma (1 - \alpha T_r) \quad (3-29)$$

Set $T_r = 313K$, $T_0 = 12$, $\alpha = 0.00183$, $\theta_0 = 12$, $b = 16$; $R = 0.114m$, $Y = 0.150m$, $A = 0.060m$, $D = 0.015m$, then $\lambda = 1.3158$, $\lambda' = 1.8421$, $\beta = \frac{0.015}{0.150} = 0.1$, $\beta' = \frac{0.015}{0.150 + 0.060} = 0.0714$. Magnetic force density distribution (Fig.3.8) is calculated from (3-28) and its unit is in k. The unit of all following figures is in k from (3-29).

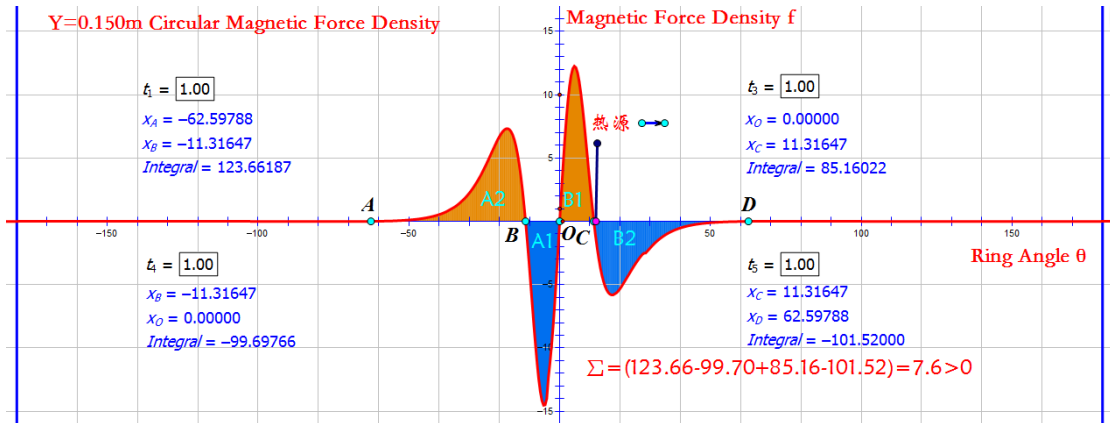


Fig. 3.8 Circular Magnetic Force Density Distribution on SMAR at $Y=0.150m$

In Fig. 3.8, Sum of areas of A_1 , A_2 , B_1 and B_2 are positive, this indicates total torque is counter clockwise.

3.4.2 Total Magnetic Force on SMAR with different Y.

Set $T_r = 313K$, $T_0 = 12$, $\alpha = 0.00183$, $\gamma = 777$, $\theta_0 = 12$, $b = 16$; $R = 0.114m$, $A = 0.060m$, $D = 0.015m$.

Without change of above parameters, we calculated total magnetic force on SMAR at $Y = 0.150m$, $Y = 0.155m$, $Y = 0.160m$, $Y = 0.165m$, $Y = 0.170m$, $Y = 0.175m$ and $Y = 0.180m$. Total magnetic force (torque) changed directions with changing Y. Calculation results of total magnetic force with k as unit are below.

Y(m)	0.150	0.155	0.160	0.165	0.170	0.175	0.180
Relative Torque	7.6	2.5	0.62	0.040	-0.12	-0.14	-0.11

Here we listed out magnetic force density distribution graph around zero. First is at $Y = 0.155m$:

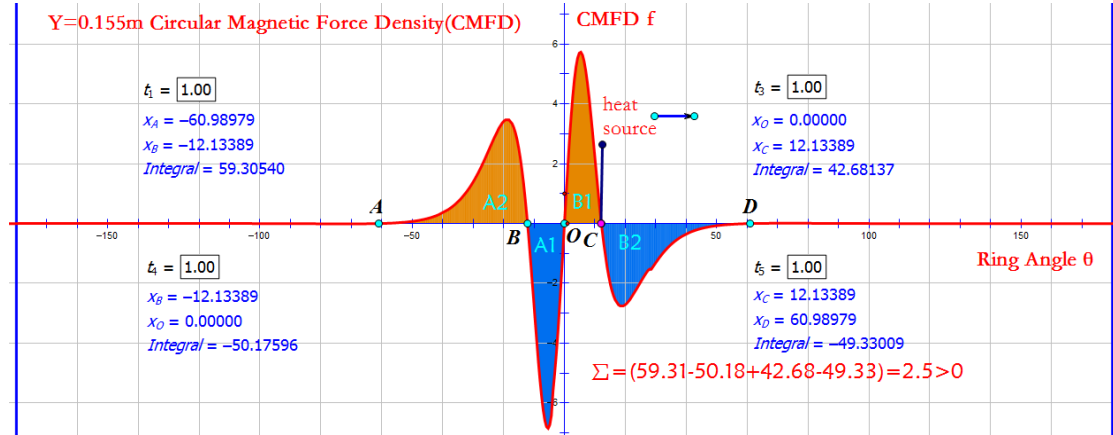


Fig.3.9 Circular Magnetic Force Density Distribution on SMAR at $Y=0.155m$

When $Y = 0.155m$, its magnetic force density distribution is shown in Fig. 3.9. Total sum of four areas A_1 , A_2 , B_1 and B_2 is positive, that is, $(S_{A_2} + S_{B_1}) - (S_{A_1} + S_{B_2}) > 0$. SMAR has total torque that is counter clockwise. When total torque is greater than friction and other resistance torque, SMAR drives by counter clockwise torque, and starts to rotate counter clockwise.

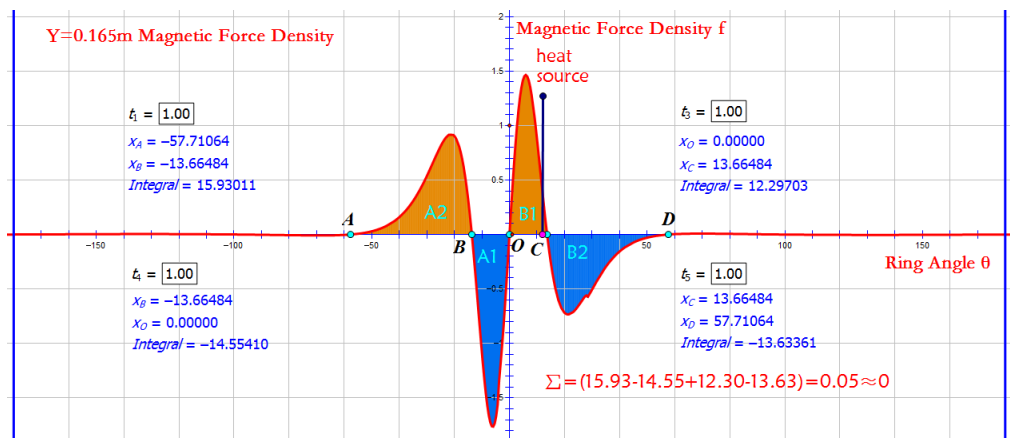


Fig.3.10 Circular Magnetic Force Density Distribution on SMAR at $Y=0.165m$

When $Y = 0.165m$, its magnetic force density distribution is shown in Fig. 3.10. Total sum of four areas A_1 , A_2 , B_1 and B_2 is close to zero, that is, $(S_{A_2} + S_{B_1}) - (S_{A_1} + S_{B_2}) \approx 0$. SMAR has total torque that is counter clockwise, but

fairly small. When total torque is less than friction and other resistance torque, SMAR remains stationary, and does not rotate.

Total magnetic force is even closer to zero at $Y = 0.166m$. Its magnetic force density distribution is as shown in Fig.3.11.

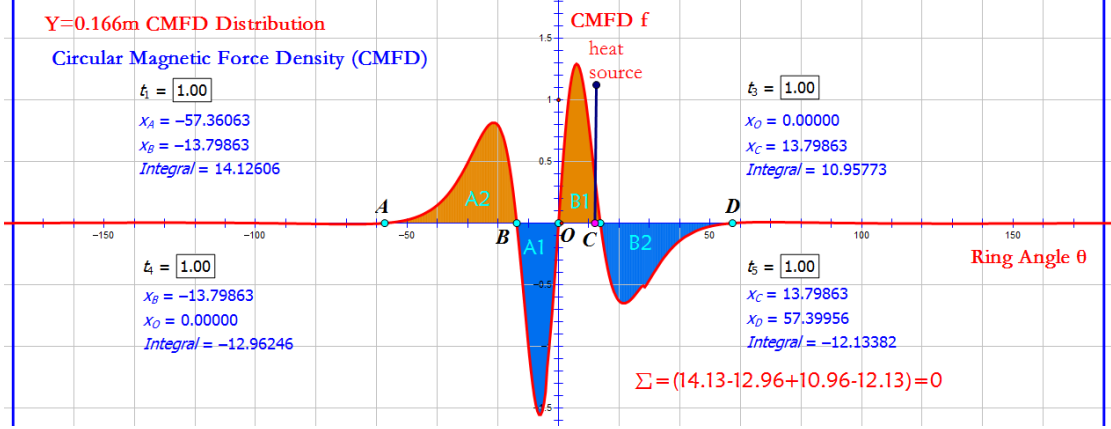


Fig.3.11 Circular Magnetic Force Density(CMFD) Distribution on SMAR at $Y=0.166m$

When $Y > 0.166m$, total magnetic force changes directions. Fig.3.12 is calculation result at $Y = 0.175m$.

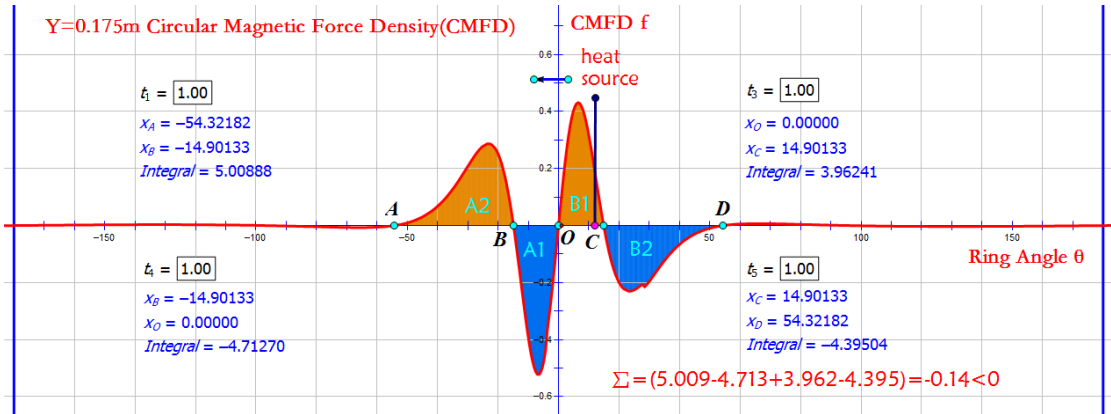


Fig. 3.12 Circular Magnetic Force Density(CMFD) Distribution on SMAR at $Y=0.175m$

When $Y = 0.175m$, its magnetic force density distribution is shown in Fig. 3.12. Total sum of four areas A_1 , A_2 , B_1 and B_2 is negative, that is, $(S_{A_2} + S_{B_1}) - (S_{A_1} + S_{B_2}) < 0$. SMAR has total torque that is clockwise. When total torque is greater than friction and other resistance torque, SMAR drives by clockwise torque, and starts to rotate clockwise.

From above, algebra sum of area of A_1 , A_2 , B_1 and B_2 $\Sigma = (S_{A_2} + S_{B_1}) - (S_{A_1} + S_{B_2})$ can change between positive and negative. Regions of A_2, B_1 are above horizontal axis, represents counter clockwise force on SMAR. Regions of A_1, B_2 are below horizontal axis, represents clockwise force on SMAR. Sum of all

area above decides the final rotation direction of SMAR.

With fixed heat source, with magnet position changes, when $(A_2+B_1)-(A_1+B_2) > 0$, SMAR rotates counter clockwise. When $(A_2+B_1)-(A_1+B_2) = 0$, SMAR does not rotate. When $(A_2+B_1)-(A_1+B_2) < 0$, SMAR rotates clockwise.

Chapter IV SMAR Kinetic Experiment and Data Fitting

4.1 Measurement and Analysis of Magnetic Field on SMAR Generated by Magnet

Based on schematic of circular magnetic field, Fig 2.2, marks non-metallic base platform to 16 equal parts (each covers $\frac{\pi}{16}$). Place magnet at a fixed place away from the base platform (distance = Y – R, use 10mm and 20mm respectively). Set the point directly opposite to magnet as origin, use Tesla meter to measure along tangent of base platform. Measurement results are shown in table 4.1. After first round of testing results, switch magnetic N and S, a comparative test results are obtained and shown in table 4.2. Measurement results indicates that switching pole does not have significant effect on results. Because of this, results in table 4.1 are used in analysis and fitting with theoretical modeling.

Table 4.1 Measurement Results of Circular Magnetic Field (mT) by Magnet (N)

Angle D \ Angle	$-\frac{5\pi}{16}$	$-\frac{\pi}{4}$	$-\frac{3\pi}{16}$	$-\frac{\pi}{8}$	$-\frac{\pi}{16}$	0	$\frac{\pi}{16}$	$\frac{\pi}{8}$	$\frac{3\pi}{16}$	$\frac{\pi}{4}$	$\frac{5\pi}{16}$
10mm	-3	-5	-11	-27	-86	0	81	21	8	6	2
20mm	-3	-5	-10	-22	-40	0	46	18	7	6	2

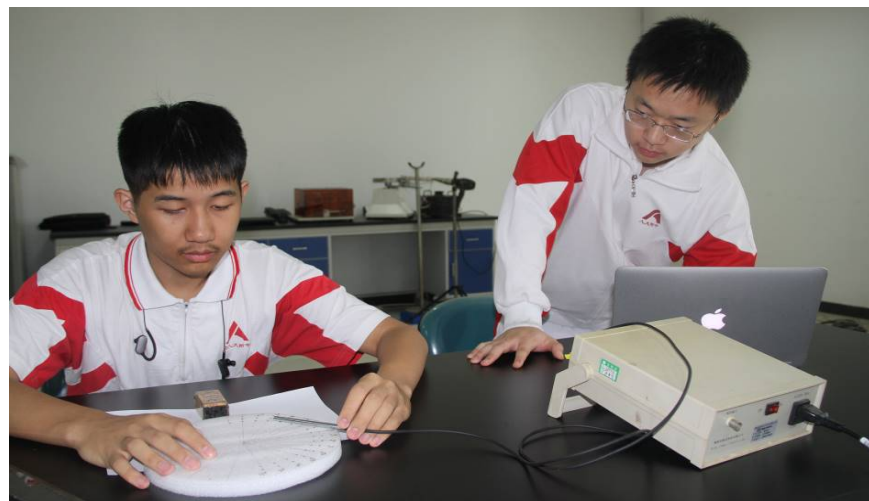


Fig.4.1 Circular Magnetic Field Measurement

In Chapter III, we derived circular magnetization distribution equation (3-17)

$$H_\theta(\theta) = \frac{M_p S_p}{4\pi R^2} [\Phi(\lambda, \theta) - \Phi(\lambda', \theta)]$$

In which,

$$\Phi(\lambda, \theta) = \frac{1}{2\beta\lambda^2} \left[\frac{2 + \lambda^2 - 2\lambda \cos(\theta + \beta)}{\sqrt{1 + \lambda^2 - 2\lambda \cos(\theta + \beta)}} - \frac{2 + \lambda^2 - 2\lambda \cos(\theta - \beta)}{\sqrt{1 + \lambda^2 - 2\lambda \cos(\theta - \beta)}} \right]$$

$$\Phi(\lambda', \theta) = \frac{1}{2\beta'\lambda'^2} \left[\frac{2 + \lambda'^2 - 2\lambda' \cos(\theta + \beta')}{\sqrt{1 + \lambda'^2 - 2\lambda' \cos(\theta + \beta')}} - \frac{2 + \lambda'^2 - 2\lambda' \cos(\theta - \beta')}{\sqrt{1 + \lambda'^2 - 2\lambda' \cos(\theta - \beta')}} \right]$$

$\Phi(\lambda, \theta)$ and $\Phi(\lambda', \theta)$ are pure factor. (3-17) can be rewritten to:

$$B_\theta(\theta) = \mu_0 H_\theta(\theta) = \frac{\mu_0 M_p S_p}{4\pi R^2} [\Phi(\lambda, \theta) - \Phi(\lambda', \theta)] \quad (4-1)$$

In which $B_\theta(\theta)$ is circular magnetic flux density which is measured in table 4.1. Thus measured results can be used to compare with calculation results in (4-1). See fig. 4.2 and 4.3, whereas, fig 4.2 showed when distance is 0.01m, that is $Y = 0.124m$. Fig 4.3 represents when distance is 0.02m, that is $Y = 0.134m$.

At $Y = 0.124m$

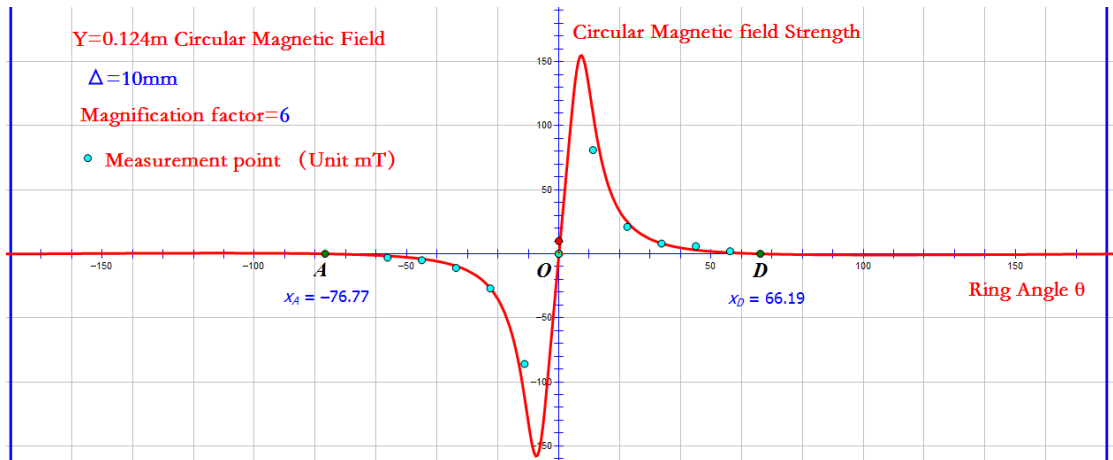


Fig. 4.2 Circular Magnetic Field Experimental Data and Calculated Curve comparison.

Experimental data means that factor $\frac{\mu_0 M_p S_p}{4\pi R^2} = 6(mT)$ in (4-1)

$$\mu_0 M_p = 6 \cdot \frac{4\pi R^2}{S_p}$$

Put $R = 0.114m$, $S_p \approx 0.0009m^2$ into above equation:

$$\mu_0 M_p = 1088mT = 1.088T$$

Comparison at $Y = 0.134m$ is below:

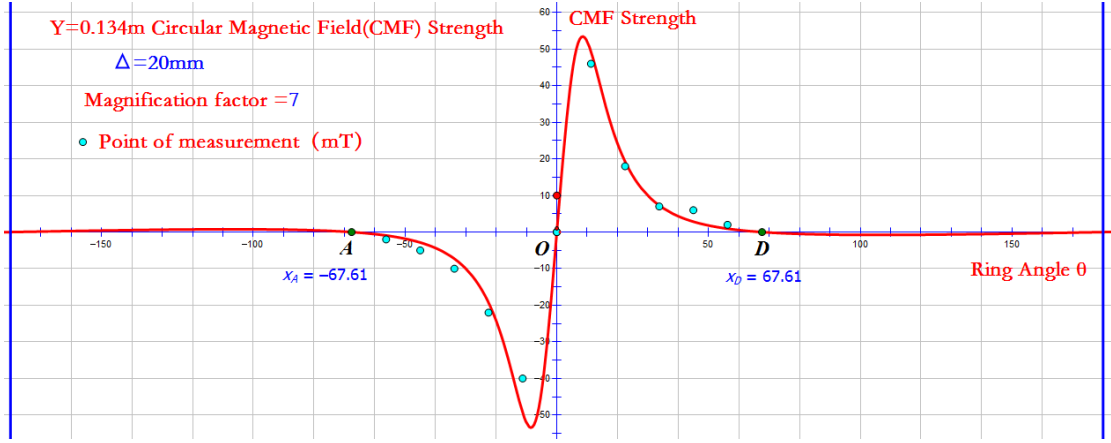


Fig. 4.3 Circular Magnetic Field Experimental Data and Calculated Curve comparison at
 $Y=0.134m, \Delta=0.02m$

Experimental data means that factor $\frac{\mu_0 M_p S_p}{4\pi R^2} = 7(mT)$ in (4-1)

$$\mu_0 M_p = 7 \cdot \frac{4\pi R^2}{S_p}$$

Put $R = 0.114m$, $S_p \approx 0.0009m^2$ into above equation:

$$\mu_0 M_p = 1269mT = 1.269T$$

Remanence B_r in common Nd-Fe-B magnets is B value that corresponding to $H = 0$, which is $\mu_0 M$. Product properties listed $B_r = 1.1 \sim 1.5T$. This property is consistent with our calculation. This also supports the validity of our theoretical calculation.

4.2 Measurement and Analysis of Magnetization and Temperature Relation on SMAR



Fig 4.4 Measurement Procedure of Magnetic Materials Magnetization at Different Temperature
Utilize NIM-2000S SMAR DC magnetization measurement system to measure magnetization of SMAR at different temperature (Fig. 4.4),

Table 4.2 Measurement Results of Magnetic Polarization $\mu_0 M_s$ (T) of SMAR Material at Various Temperatures (Celsius)

°C	24	40	60	80	100	130	160	190	200
$\mu_0 M_s$	1.324	1.293	1.239	1.176	1.041	0.887	0.715	0.477	0.276

Changes the temperature to Kelvin, magnetic polarization uses mT to get Table 4.3.

Table 4.3 Measurement Results of Magnetic Polarization $\mu_0 M_s$ (mT) of SMAR Material at Various Temperatures (Kelvin)

K	297	313	333	353	373	403	433	463	473
$\mu_0 M_s$	1324	1293	1239	1176	1041	887	715	477	276

Draw a graph (Fig. 4.5) from table 4.3. Magnetic polarization and temperature are appropriate linear in relation. With linear curve fitting, function is:

$$\mu_0 M = 3124 - 5.72T \quad (4-2)$$

Linear correlation coefficient is $r = -0.978$.

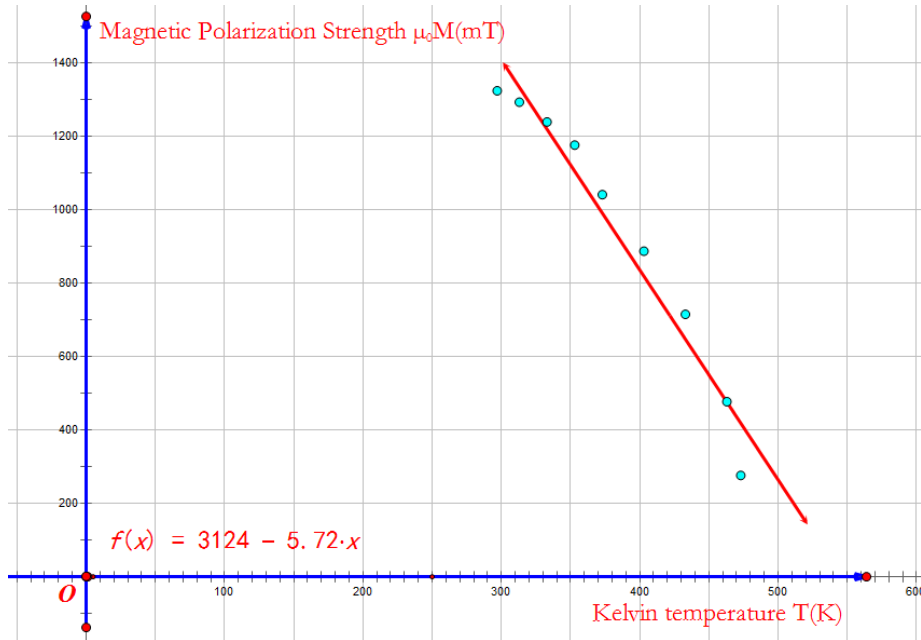


Fig.4.5. Measurement on Magnetic Polarization and Temperature Relations

Based on susceptibility definition, bring (4-2) in:

$$\chi(T) = \frac{\mu_0 M}{\mu_0 H} = \frac{3124}{\mu_0 H} \left(1 - \frac{5.72}{3124} T \right) = \chi_0 \left(1 - 0.00183 T \right) \quad (4-3)$$

Bring $\mu_0 H = 4\pi \times 10^{-7} \times 3200 \times 1000 \text{ (mT)} = 4.02 \text{ (mT)}$ into (4-3):

$$\chi_0 = \frac{3124}{4.02} = 777$$

With linear regression, relative susceptibility and temperature are approximates to:

$$\chi(T) = 777 \left(1 - 0.00183 T \right) \quad (4-4)$$

Since soft magnetic material's susceptibility is influenced by complex action and interaction of magnetic field, temperature, stress etc., to simplify the analysis, magnetic fields factor on susceptibility and temperature relation (4-4) is used to represent susceptibility's approximation at certain magnetic field range and temperature range ($T=297-473\text{K}$).

4.3 Measurement and Analysis of SMAR Temperature Distribution

Based on measurement method from Chapter II, a measurement platform is constructed. SMAR is fixed on non-magnetic alloy plate and marked to 60 equal parts (every 6°). Remove magnet, place thermometer at a fix location from SMAR. Data is

collected by rotating SMAR's specific measurement location to the effective measurement range. Once data is obtained, rotate the measurement point to its original location. Apply heat for 30s to stable to start measurement for next data point (Fig.4.6). Repeat above steps, measure 57degree on either side of fixed heat source to obtain SMAR temperature gradient distribution, listed in Table 4.4.



Fig.4.6 During SMAR Temp Measurement

Table 4.4 SMAR Temperature Distribution Measurement Results

θ (°)	-57	-51	-45	-39	-33	-27	-21	-15	-9	-3
T (°C)	48.4	49.3	49.6	51.9	51.9	57.6	61.5	85.8	95.8	101.9
θ (°)	3	9	15	21	27	33	39	45	51	57
T (°C)	100.7	98.5	89.1	66.3	53.1	52.0	51.4	49.3	50.1	48.2

Based on analyze of measurement results, fits with SMAR temperature distribution (4-5), arrives (Fig.4.7). Fitted results are $b = 16^\circ$, $T_r = 40^\circ C$, that is $T_r = 313K$ (4-6) .

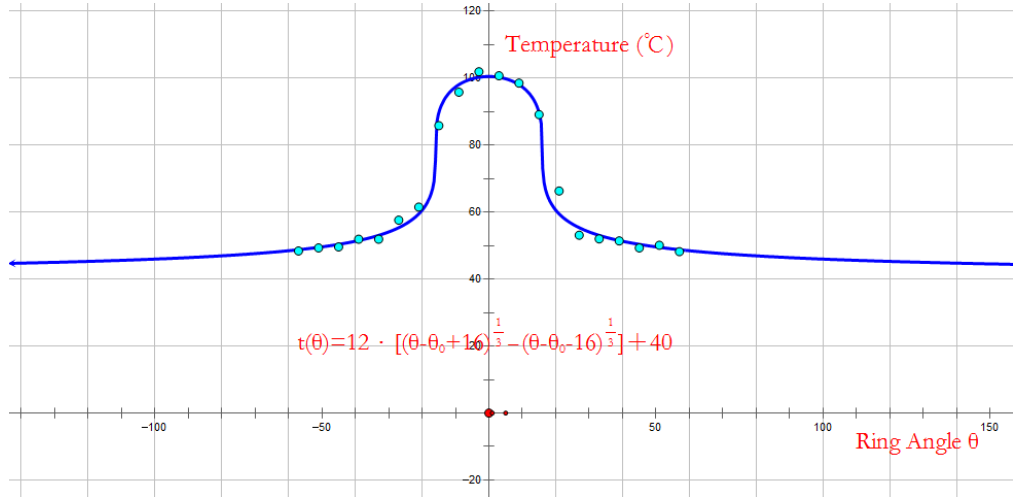


Fig.4.7 Fitted curve of SMAR Temperature Distribution
Measurement and Calculated Results

Temperature on locally heated SMAR is measured. Single peak temperature distribution is obtained. Temperature curve is symmetrical to the position of heat source. Further away from heat source, temperature tends to a consistent value.

Through analysis, using a monolithically decreasing function that is symmetrical and tend to zero further away. Such a function with background temperature is a good approximation to the experimental data. Fitted function is (in Kelvin):

$$T(\theta) = T_0 \left[(\theta + b)^{\frac{1}{3}} - (\theta - b)^{\frac{1}{3}} \right] + T_r \quad (4-5)$$

In which, T_r is background temperature, or environment temperature.

$$T(\theta) = 12 \cdot \left[(\theta - \theta_0 + 16)^{\frac{1}{3}} - (\theta - \theta_0 - 16)^{\frac{1}{3}} \right] + 313 \quad (4-6)$$

4.4 Motion Observation and Analysis for SMAR with Thermo-Magnetic Interaction

This section describes experimental verification of modeling from chapter III that clockwise, counter clockwise and stationary around the critical points based on magnet distance Y. To control other factors effects on the experiments, only magnet's location in relative to center of SMAR Y changes, other parameters remains the same.

4.4.1 SMAR's Motion Observation and Analysis with Magnet at Y=0.175m

With platform constructed and parameter sets, measurement and record distance

between center of SMAR and magnet pole, Y. Observed at Y=0.175m, experiment process are recorded with video and photos, (Fig.4.8). After measurement, stop heat source and platform cools to room temperature.

In the experiment, we observed that with fixed heat source applied for some time, platform starts to rotate clockwise. Fig.4.9 shows curve. X-axis is circular angle; total magnetic force is calculated to be negative. The platform rotates clockwise.



Fig. 4.8 Clockwise rotation of the Platform

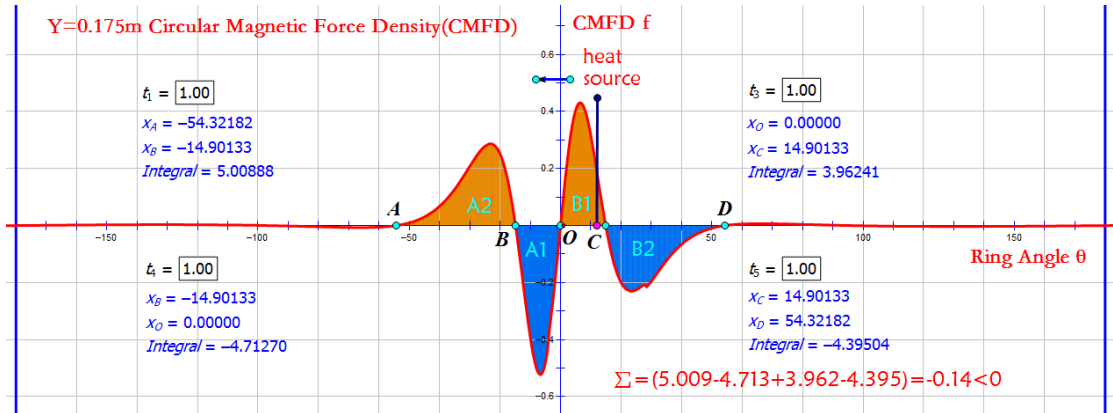


Fig. 4.9 Circular Magnetic Force Density(CMFD) Distribution at Y = 0.175m

Fig 4.9, horizontal axis is circular angle. Area of four parts are $S_{A_2} = 5.009$, $S_{A_1} = 4.713$, $S_{B_1} = 3.962$, $S_{B_2} = 4.395$. Total magnetic force is $F = (S_{A_2} + S_{B_1}) - (S_{A_1} + S_{B_2}) = -0.14$, the results is negative. This means that total torque on SMAR is clockwise. SMAR rotates clockwise. This is consistent with our experimental observation.

4.4.2 SMAR's Motion Observation and Analysis with Magnet at Y=0.165m

Adjusting Y to Y=0.165m. Applying heat with fixed heat source for 5 mins, SMAR

remains stationary, Fig.4.10. Heating stops and let rotation platform cool to room temperature. Total force on SMAR is calculated, and results are shown in Fig.4.11.



Fig. 4.10 Rotation Platform Remains Stationary at Y=0.165m

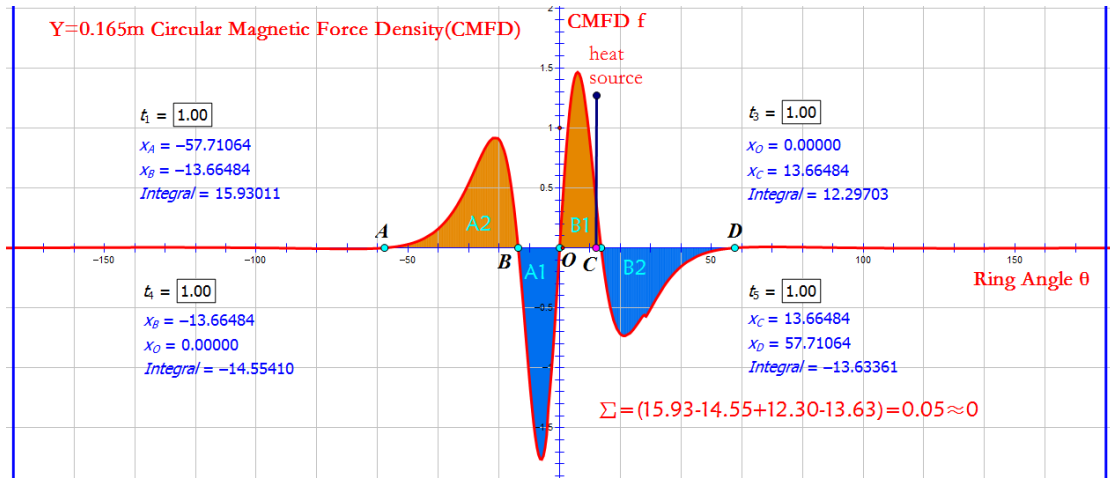


Fig. 4.11 Circular Magnetic Force Density (CMFD) Distribution at Y = 0.165m

In Fig.4.11, Area of four parts are $S_{A2} = 15.93$, $S_{A1} = 14.55$, $S_{B1} = 12.30$,

$S_{B2} = 13.63$. Total magnetic force is $F = (S_{A2} + S_{B1}) - (S_{A1} + S_{B2}) = 0.05 \approx 0$, the results close to zero. Since the experimental apparatus has frictions, the magnetic force cannot overcome the friction. SMAR does not move. This is also consistent with our experimental observation.

4.4.3 SMAR's Motion Observation and Analysis with Magnet at Y=0.155m

Adjusting Y to Y=0.155m. Applying heat with fixed heat source for 5 mins, SMAR starts to rotate counter clockwise. Experimental process is recorded with video and photography. Fig.4.12 Total force on SMAR is calculated, and results are shown in Fig.4.13.



Fig. 4.12 Platform rotates Counter Clockwise

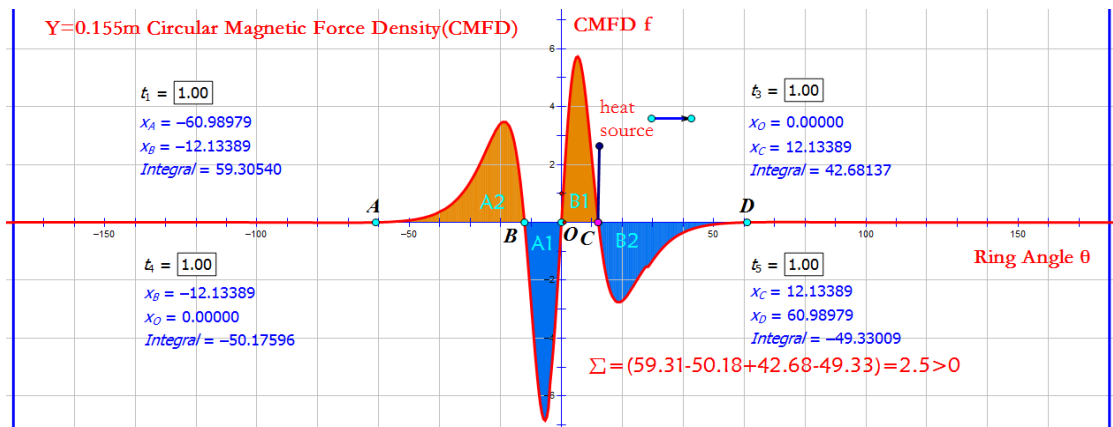


Fig. 4.13 Circular Magnetic Force Density (CMFD) Distribution at $Y = 0.155\text{m}$

In Fig.4.13, Area of four parts are $S_{A2} = 59.31$, $S_{A1} = 50.18$, $S_{B1} = 42.68$,

$S_{B2} = 49.33$. Total magnetic force is $F = (S_{A2} + S_{B1}) - (S_{A1} + S_{B2}) = 2.5 > 0$, the results is positive. This means that total torque on SMAR is counter clockwise. SMAR rotates counter clockwise. This is also consistent with our experimental observation.

Above experimental results show that force balance on SMAR is broken under thermo-magnetic interaction. SMAR starts to rotate. Direction of rotation is closely related to distance of magnet to SMAR's center. The distance change from 0.175m to 0.165m, SMAR changes from rotation clockwise to no movement; further reduce the distance, SMAR rotates counter clockwise. With decreasing Y , zero-point C of the curve has moved to left side of heat source in Fig.4.13. At the same time, SMAR has changed from rotation clockwise, stationary and counter clockwise.

The above observation from SMAR movement experiment verified the motion model established in Chapter III as well as pattern of movement. This proves that the motion model of SMAR and pattern of movement as a result of analysis are correct and reliable under considered conditions.

Chapter V Conclusion and Future Study

- Starting from the classic electro-magnetic theory, the circular magnetic field intensity distribution equation along the SMAR is established. From here, the circular magnetic field intensity gradient distribution equation along the SMAR can be acquired.

1.1 The circular magnetic field intensity distribution equation along the SMAR:

$$H_\theta(\theta) = \frac{M_p S_p}{4\pi R^2} [\Phi(\lambda, \theta) - \Phi(\lambda', \theta)]$$

In which

$$\Phi(\lambda, \theta) = \frac{1}{2\beta\lambda^2} \left[\frac{2 + \lambda^2 - 2\lambda \cos(\theta + \beta)}{\sqrt{1 + \lambda^2 - 2\lambda \cos(\theta + \beta)}} - \frac{2 + \lambda^2 - 2\lambda \cos(\theta - \beta)}{\sqrt{1 + \lambda^2 - 2\lambda \cos(\theta - \beta)}} \right]$$

$$\Phi(\lambda', \theta) = \frac{1}{2\beta' \lambda'^2} \left[\frac{2 + \lambda'^2 - 2\lambda' \cos(\theta + \beta')}{\sqrt{1 + \lambda'^2 - 2\lambda' \cos(\theta + \beta')}} - \frac{2 + \lambda'^2 - 2\lambda' \cos(\theta - \beta')}{\sqrt{1 + \lambda'^2 - 2\lambda' \cos(\theta - \beta')}} \right]$$

1.2 The circular magnetic field intensity gradient distribution equation:

$$\frac{1}{R} \frac{\partial H_\theta(\theta)}{\partial \theta} = \frac{M_p S_p}{4\pi R^3} [G(\lambda, \theta) - G(\lambda', \theta)]$$

- Based on conclusion 1, the circular magnetic force density distribution equation along the SMAR is derived:

$$f_\theta(\theta) = k\chi [\Phi(\lambda, \theta) - \Phi(\lambda', \theta)] [G(\lambda, \theta) - G(\lambda', \theta)]$$

- Curves of circular distribution of temperature along the SMAR and the relation between magnetic polarization strength and temperature are fitted out from experimental data.

3.1 Circular distribution of temperature along SMAR (in Kelvin):

$$T(\theta) = 12 \cdot \left[(\theta - \theta_0 + 16)^{\frac{1}{3}} - (\theta - \theta_0 - 16)^{\frac{1}{3}} \right] + 313$$

3.2 Relation between the magnetic polarization strength and temperature:

$$\mu_0 M = 3124 - 5.72T$$

- Based on conclusion 3, the circular distribution curve of relative susceptibility along the SMAR is derived:

$$\chi(\theta) = 332 \left\{ 1 - 0.0514 \left[(\theta - \theta_0 + b)^{\frac{1}{3}} - (\theta - \theta_0 - b)^{\frac{1}{3}} \right] \right\}$$

5. Based on conclusion 2 and 4, we finally establish the motion model of SMAR under the actions of both magnetic field and temperature gradient, which can be shown schematically in Fig.5.1.

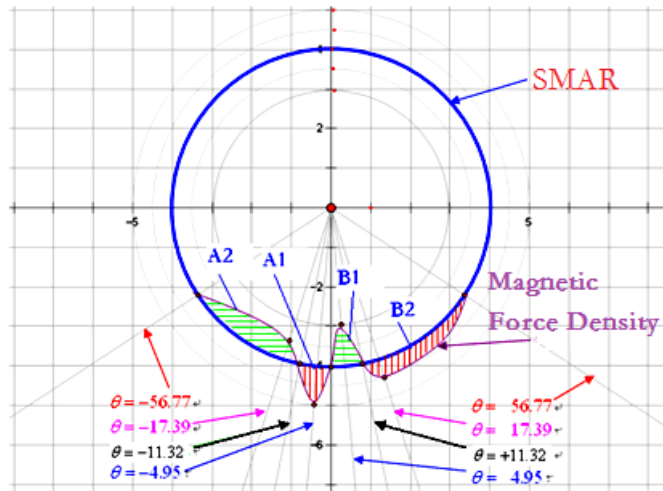


Fig.5.1 Schematic drawing of motion model of SMAR based on circular magnetic force density distribution along SMAR

As shown in Fig.5.1, the forces indicated by the areas of A2 and B1 make the SMAR rotate counter clockwise and hence, the forces indicated by those of A1 and B2 make the SMAR rotate clockwise. When $(A_2+B_1) - (A_1+B_2) > 0$, SMAR rotates counter clockwise; When $(A_2+B_1) - (A_1+B_2) = 0$, SMAR does not rotate; When $(A_2+B_1) - (A_1+B_2) < 0$, SMAR rotates clockwise.

6. From conclusion 5, we discovered two novel phenomena. The first one is that on each side of the symmetric line (magnet), there are at least two force applied on the SMAR with opposite directions (clockwise and counter clockwise), and it overturns our intuitive understanding. The second one is that a SMAR can rotate either counter clockwise or clockwise when the distance between the magnet and the SMAR changes, and once again it overturns our intuitive understanding.
7. According to calculation, when $Y=0.175m$, SMAR rotates clockwise; when $Y=0.165m$, SMAR does not rotate; when $Y=0.155m$, SMAR rotates counter clockwise. Experimental results support the above theoretical analysis.
8. The most hopeful application of this work will be in the field of new energy, as shown in Fig.5.2. Sunlight focused on black painted SMAR after going through

convex lens. SMAR's temperature rises after absorbing heat from sunlight, generating temperature gradient. This results in loss of balance of magnetic force and the SMAR starts rotating. This apparatus can directly convert solar energy into mechanical energy. This device may be a high efficiency and clean energy solution.

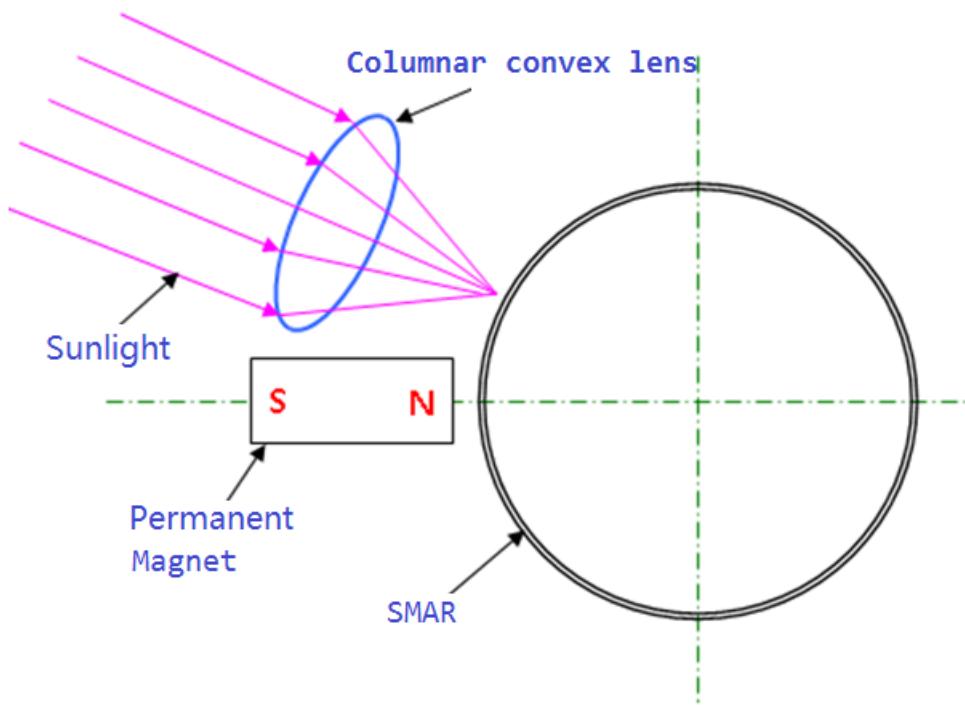


Fig. 5.2 Schematic of theory of future work

Appendix. Table of Physics Units and Signs

Sign	Name	Unit Name	Unit Sign
M	Magnetization	安培·米 ⁻¹	$A \cdot m^{-1}$
μ_0	Vacuum permeability	亨利·米 ⁻¹	$H \cdot m^{-1}$
H	Magnetic Field Strength	安培·米 ⁻¹	$A \cdot m^{-1}$
B	Magnetic Flux Strength	特斯拉	T
T	Kelvin	开尔文	K

Bibliography

- [1] J. F. Elliott. Thermomagnetic Generator. Journal of Applied Physics, 1959, 30(11):1774-1777
- [2] Efficiency of Thermomagnetic Generator, Journal of Applied Physics, 1959, 30:1622-1623
- [3] K. Murakami. The Characteristics of Ferrite Cores with Low Curie Temperature and their Application. IEEE Transactions on Magnetics 1965,(2): 96-100
- [4] L.D.Kirol, J.I.Mills. Numerical analysis of thermomagnetic generator. Journal of Applied Physics, 1984, 56(3): 824-828
- [5] 李东辉,罗二仓,吴张华,戴巍.一种新型的发电方式—热磁发电研究.中国工程热物理学会学术会议论文.
- [6] 瞿清昌,王京平,林安利,李之彬. 磁性材料自动测量装置的研究.第十届全国磁学和磁性材料会议.1999年, 689-690
- [7] 赵凯华,陈熙谋.《电磁学》(上册).第1版,第1章: 静电场§1静电的基本现象和基本规律.
- [8] 赵凯华,陈熙谋.《电磁学》(下册).第1版,第6章:磁介质§2等效磁荷观点.

Acknowledgement

This study is completed under careful guidance of Mr. Yongping Zhang, teacher at High School Affiliated to Renming University. His rigorous style set a good example for us. During the investigation, Lansong Li was in charge of selecting the topic, design and implemented experiments, model creation and drafting of the paper; Junning Zhao participated model creation, experiments and portion of paper drafting.

Thanks to Baogang Song, who provided part of experimental material such as soft magnetic alloy ring, magnetic measurement equipment. This allowed us to complete our experiments and achieved desired results.

Thanks to our parents. Their understanding and support of our investigation is our main driving force.

This participating team declare that submitted paper is result of research under the guidance of supervision teacher. To the best of knowledge of the team, this article does not include any work published or written by others. The team will take responsibility of any false information.

Team Member: _____

Supervising Teacher: _____

Date:

本参赛团队声明所提交的论文是在指导老师指导下进行的研究工作和取得的研究成果。尽本团队所知，除了文中特别加以标注和致谢中所罗列的内容以外，论文中不包含其他人已经发表或撰写过的研究成果。若有不实之处，本人愿意承担一切相关责任。

参赛队员： 李良松 赵俊宁 指导老师：张永年

2018 年 9 月 7 日